

## Plasma Relativistic Microwave Electronics

M. V. Kuzelev, O. T. Loza, A. A. Rukhadze, P. S. Strelkov, and A. G. Shkvarunets

*Institute of General Physics, Russian Academy of Sciences, ul. Vavilova 38, Moscow, 119991 Russia*

Received March 22, 2001

**Abstract**—The principles of plasma relativistic microwave electronics based on the stimulated Cherenkov emission of electromagnetic waves in the interaction of a relativistic electron beam with a plasma are formulated. A theory of relativistic Cherenkov plasma microwave oscillators and amplifiers is developed, and model experimental devices are elaborated and investigated. The emission mechanisms are studied theoretically. The efficiencies and frequency spectra of relativistic Cherenkov plasma microwave oscillators and amplifiers are calculated. The theoretical predictions are confirmed by the experimental data: the power of the devices attains 500 MW, the microwave frequency can be continuously tuned over a wide band with an upper-to-lower boundary frequency ratio of 7 (from 4 to 28 GHz), and the emission frequency bandwidth can be varied from several percent to 100 percent. These microwave sources have no analogs in microwave electronics. © 2001 MAIK “Nauka/Interperiodica”.

### 1. INTRODUCTION

#### 1.1. The Subject of Plasma Relativistic Microwave Electronics

Microwave electronics is one of the main branches of physical electronics—an extensive (fundamental and applied) science. The subjects of investigation of microwave electronics are oscillations and waves in the frequency band 1–100 GHz, the methods for their excitation by electron beams, and many practical applications.

Since a plasma consists of charged particles (electrons and ions), it is subject to numerous natural oscillations precisely in the microwave frequency range. For this reason, a device filled with plasma may serve as a source of microwave radiation.

There are two types of plasma-filled microwave sources. Devices of the first type are conventional vacuum microwave sources filled with plasma. Filling a vacuum source with plasma makes it possible to improve some of its parameters (to increase the microwave power, to change the frequency, etc.). Such sources were called *hybrid* microwave devices. Since the mechanism for microwave excitation in hybrid devices is essentially the same as that in vacuum analogs (backward-wave tubes, gyrotrons, etc.), they can also operate in plasma-free modes. That is why such hybrid devices are not a significant concern for plasma microwave electronics.

Plasma-filled devices of the second type are based on the resonant interaction of an electron beam with a plasma. This interaction leads to the excitation of eigenmodes of plasma-filled systems (plasma waveguides or plasma resonators), which cannot be excited in the absence of plasma. For this reason, such sources were called *plasma* microwave devices. Plasma microwave electronics is primarily concerned with the

mechanisms for microwave excitation (emission) by an electron beam in plasma systems and the creation of related plasma microwave devices. Accordingly, plasma microwave devices and their physical justification are the focus of our investigation.

Considerable progress in plasma microwave electronics is associated with the development of methods for generating relativistic electron beams (REBs) (i.e., beams in which the electron velocity is close to the speed of light). In a plasma, REBs excite electromagnetic waves with relativistic phase velocities. Plasma microwave electronics dealing with REBs was called relativistic.

Below, we will review the results obtained in studies on plasma relativistic microwave electronics. We also formulate the general principles underlying this new area of modern physics, survey the relevant theoretical and experimental advances, and discuss the prospects of plasma relativistic microwave devices as well as their possible practical applications.

#### 1.2. Historical Review

The beam–plasma instability was discovered as early as 1949 by A.I. Akhiezer and Ya.B. Fainberg [1] and independently by D. Bohm and E. Gross [2]. Further research on this instability gave birth to plasma microwave electronics. Physically, the beam–plasma instability consists in an anomalously strong interaction of a fast electron beam with a dense plasma. The theory predicted that a monoenergetic electron beam should be fairly efficiently decelerated by a plasma, thereby giving rise to plasma oscillations. In a spatially unbounded beam–plasma system, the characteristic time scale on which an electron beam is decelerated has the form

$$\tau = 1/\delta, \quad \delta = \omega_p(n_b/2n_p)^{1/3}. \quad (1.2.1)$$

Here,  $n_b$  and  $n_p$  are the electron densities of the beam and plasma, respectively (it is assumed that  $n_b \ll n_p$ );  $\omega_p$  is the Langmuir frequency of the plasma electrons; and  $\delta$  is the temporal growth rate of the beam instability. The characteristic distance  $l$  over which the beam electrons are decelerated is approximately equal to  $l \approx u\tau = u/\delta$ , where  $u$  is the electron beam velocity.

The growth rate  $\delta$  and, accordingly, the deceleration distance  $l$  are achieved when the frequency  $\omega$  of the excited plasma waves satisfies the condition

$$\omega \approx \omega_p \approx ku, \quad (1.2.2)$$

i.e., when the phase velocity of the plasma wave is close to the beam velocity. Here,  $k$  is the projection of the wave vector of the plasma wave onto the propagation direction of the beam. Condition (1.2.2) made it possible to understand the mechanism for the anomalously strong interaction of a dense electron beam with a plasma as being due to the stimulated emission of plasma waves by the beam electrons (stimulated Cherenkov effect). As a result, the beam kinetic energy is converted into the energy of plasma waves. The conversion efficiency  $Q$ , which can also be regarded as the emission efficiency of plasma waves by an electron beam, is estimated to be

$$Q = \left( \frac{E^2}{8\pi} \right) / \left( n_b \frac{mu^2}{2} \right) \approx \left( \frac{n_b}{2n_p} \right)^{1/3}; \quad (1.2.3)$$

where  $E^2/8\pi$  is the field energy in a plasma wave and  $mu^2/2$  is the kinetic energy of a beam electron. This estimate implies that, for  $n_b \approx 0.01n_p$  and  $u \approx 10^{10}$  cm/s (which corresponds to a beam electron energy of about 30 keV), the fraction of the beam energy that can be converted into the energy of plasma waves amounts to 20%. If, in addition,  $n_p \approx 10^{12}$  cm<sup>-3</sup> and  $n_b \approx 10^{10}$  cm<sup>-3</sup> (which corresponds to the beam current density  $j_b \approx 15$  A/cm<sup>2</sup>), then the electron beam loses 75 kW/cm<sup>2</sup> of its initial energy; this energy loss occurs during a time interval of  $10^{-10}$  s, i.e., over a distance of about  $l \sim 1$  cm.

The first experiments in this field, which were carried out in 1960 in the Soviet Union (at the Kharkov Institute of Physics and Technology [3] and the Vekua Institute of Physics and Technology [4]) and abroad confirmed that the efficiency of a collective interaction of the electron beam and the plasma is fairly high. On the other hand, electromagnetic radiation emitted from the plasma turned out to be insignificant: the fraction of the beam energy lost in the form of microwaves was smaller than 1%.

Investigation of the general properties of the beam-plasma instability was followed by research on the possibility of creating microwave emitters based on this instability, thereby marking the beginning of plasma nonrelativistic microwave electronics. Significant contributions to this scientific direction were made by the physicists of the Institute of Radio Engineering and Electronics of the Russian Academy of Sciences, who

published the first review [5] on plasma nonrelativistic microwave electronics. This review, as well as review [6], demonstrated that it is possible to excite different modes of the plasma waveguide by an electron beam and thus to create the relevant Cherenkov plasma microwave oscillators and amplifiers.

A serious difficulty in creating effective plasma microwave emitters is associated with the development of a system for transforming a slow plasma wave into a fast mode of a vacuum waveguide. The most difficult point in this way is that of making the device broadband. That is why it was impossible to make use of an important advantage of plasma microwave devices over vacuum ones—the possibility of tuning the radiation frequency over a broad band by varying the plasma density. As a result, plasma microwave devices driven by nonrelativistic electron beams have not been implemented in practice.

The situation in plasma microwave electronics changed drastically by the early 1970s, when, first, encouraging theoretical results were obtained and, then, scientists learned to produce high-current REBs with current densities of 1–10 kA/cm<sup>2</sup> and electron energies of about 1 MeV. As the relativistic factor  $\gamma$  of the electron beam increases, the growth rate  $\delta$  of the beam instability decreases [7, 8],

$$\delta = \left( \frac{n_b}{2n_p} \right)^{1/3} \frac{\omega_p}{\gamma}, \quad \gamma = \frac{1}{\sqrt{1 - u^2/c^2}}, \quad (1.2.4)$$

and, accordingly, the relaxation length  $l \approx u/\delta$  of the beam in the plasma increases, which seems to be evidence of a weakening of the beam-plasma interaction. However, in actuality, this is not the case: it is precisely because of the longer beam relaxation length that the efficiency of the beam energy transfer to plasma waves increases up to the value [9]

$$Q \approx \frac{1}{2} \left( \frac{n_b}{2n_p} \right)^{1/3} (\gamma + 1). \quad (1.2.5)$$

Notably, for large values of  $\gamma$ , the approximate formula (1.2.5) implies that the efficiency can be on the order of unity. However, this formula is valid only when the efficiency is low. Actually, numerical experiments [10] show that the maximum conversion efficiency is usually at most 20–30%.

We should also mention two theoretical results that had an important impact on the development of plasma relativistic microwave electronics. The first is the formula for the limiting current at which an electron beam can be transported through a vacuum waveguide. In particular, in a cylindrical metal vacuum (plasma-free) waveguide, the current of a thin-walled annular beam cannot exceed the limit known as the Bogdankevich–Rukhadze current [11]

$$J_0 \approx 17 \frac{(\gamma^{2/3} - 1)^{3/2}}{\Delta_b/r_b + 2 \ln R/r_b} \text{ kA}; \quad (1.2.6)$$

where  $R$  is the waveguide radius,  $r_b$  is the mean beam radius, and  $\Delta_b$  is the beam wall thickness. The current (1.2.6) stems from the deceleration of the beam electrons by the field of their own space charge and is thus the limiting beam current for vacuum microwave devices. However, even if the electron beam current is neutralized either by the ions or by the plasma, there is another limit, which is known as the Pierce current and is governed by the condition for the beam transport to be stable [12]:

$$J_p = J_0 \left( \frac{\gamma^2 - 1}{\gamma^{2/3} - 1} \right)^{3/2} > J_0 \gamma^2. \quad (1.2.7)$$

Consequently, owing to the complete (or partial) neutralization of the beam charge, plasma-filled systems can operate with beam currents that are not attainable in vacuum microwave devices.

The second important theoretical result is the condition for exciting the eigenmodes of a plasma waveguide by an electron beam. The eigenmodes can be excited only in a sufficiently dense plasma, such that the plasma frequency  $\omega_p$  is higher than a certain threshold frequency  $\omega_{\text{thr}}$  [13]:

$$\omega_p^2 > \omega_{\text{thr}}^2 = k_{\perp p}^2 u^2 \gamma^2; \quad (1.2.8)$$

where the transverse wavenumber  $k_{\perp p}$  of the plasma wave is determined by the plasma density profile and waveguide radius (see below) [10].

The currents  $J_0$  and  $J_p$  are the characteristic limiting currents of electron beams in vacuum and plasma relativistic microwave sources, respectively. Condition (1.2.8) determines the threshold plasma density above which the plasma wave can be excited by an REB.

By 1976, the basic elements of plasma relativistic microwave electronics were comprehended in general principles [14–16]. Since that time, a long-term close collaboration between experimental and theoretical groups began, which led to the development a new branch of microwave electronics—plasma relativistic microwave electronics. Our combined efforts made it possible to devise an optimum scheme of plasma relativistic microwave sources—an annular REB and an annular plasma column in a metal waveguide with a strong longitudinal external magnetic field. We constructed linear and nonlinear theories of plasma relativistic microwave oscillators and amplifiers, investigated the emission mechanisms in these devices, and calculated the emission efficiency and emission spectra.

Our first successful experiment with a relativistic Cherenkov plasma maser (RCPM) was carried out in 1982 at the Institute of General Physics of the Russian Academy of Sciences [17, 18]. Then, the theory developed was used to design and investigate high-power Cherenkov plasma microwave oscillators and amplifiers tunable over a broad frequency band. We also elaborated new original diagnostics for measuring and controlling the parameters of high-current pulsed relativistic

electron beams and high-power microwave radiation.

## 2. THEORETICAL PLASMA RELATIVISTIC MICROWAVE ELECTRONICS

### 2.1. Linear Theory of the Plasma Relativistic Microwave Amplifier

The simplest theoretical model of a plasma microwave amplifier assumes a straight REB propagating along the axis of a plasma-filled metal waveguide of radius  $R$  in a strong longitudinal external magnetic field. The beam is injected into the waveguide through the plane  $z = 0$ . A collector is placed in the plane  $z = L$  and is coupled to the emitter (the outlet horn). The beam and plasma are homogeneous along the waveguide axis, cold, and completely charge- and current-neutralized. In the waveguide cross section, the plasma and beam are annular, with the mean radii  $r_b < R$  and  $r_p < R$  and wall thicknesses  $\Delta_b$  and  $\Delta_p$  such that  $\Delta_{b,p} \ll r_{b,p}$ .

In the linear approximation, the spectra of the natural oscillations in this waveguide system are determined from the following dispersion relation [19, 20], which is derived from Maxwell's equations, the hydrodynamic equation for a cold plasma, and the Vlasov equation for the beam electrons:

$$D_p D_b = \theta \omega_p^2 \omega_b^2 \gamma^{-3} \frac{\chi^4}{k_{\perp p}^2 k_{\perp b}^2}. \quad (2.1.1)$$

Here,

$$D_p \equiv \omega^2 - \omega_p^2 \frac{\chi^2}{k_{\perp p}^2}, \quad D_b \equiv (\omega - k_z u)^2 - \omega_b^2 \gamma^{-3} \frac{\chi^2}{k_{\perp b}^2} \quad (2.1.2)$$

are the dispersion functions, whose zeros determine the wave spectra in the plasma and electron beam, provided that they do not interact with one another [10]; parameter  $\theta$  characterizes the degree to which the beam and plasma waves are coupled; and quantities  $k_{\perp p}^2$  and  $k_{\perp b}^2$  are the squared transverse wavenumbers of the beam and plasma waves. The rest of the notation in formulas (2.1.1) and (2.1.2) is as follows:  $\omega$  is the frequency,  $k_z$  is the longitudinal wavenumber,  $\omega_p$  and  $\omega_b$  are the Langmuir frequencies of the plasma and beam electrons,  $\chi^2 = k_z^2 - \omega^2/c^2$ ,  $u$  is the unperturbed velocity of the beam electrons, and  $\gamma = (1 - u^2/c^2)^{-1/2}$  is the relativistic factor.

The coupling parameter  $\theta$  possesses an important property:  $\theta = 1$  for  $r_b = r_p$  and  $\theta < 0$  in other cases. Thus, for azimuthally symmetric low-frequency perturbations such that  $\omega R/u\gamma \ll 1$ , parameter  $\theta$  is equal to

$$\theta = \begin{cases} \ln(R/r_p)/\ln(R/r_b), & r_b < r_p, \\ \ln(R/r_b)/\ln(R/r_p), & r_b > r_p. \end{cases} \quad (2.1.3)$$

As the frequency  $\omega$  increases, the coupling parameter  $\theta$  decreases substantially in comparison with that in formula (2.1.3).

The values of  $\omega$  and  $k_z$  that are close to those at which the dispersion functions (2.1.2) vanish simultaneously correspond to a strong (single-particle or collective) Cherenkov resonance between the beam and plasma. Cherenkov resonance can occur only in the frequency range  $\omega < k_z c$ , in which the beam and plasma waves are surface waves. In particular, in the most important long-wavelength limit ( $k_z \rightarrow 0$ ), the dispersion relation for the surface plasma wave has the form [10]

$$\omega = \omega_p \frac{k_z c}{\sqrt{k_{\perp p}^2 c^2 + \omega_p^2}}, \quad (2.1.4)$$

where the squared transverse wavenumber of the plasma wave is equal to

$$k_{\perp p}^2 = \begin{cases} [r_p \Delta_p \ln(R/r_p)]^{-1}, & l = 0, \\ 2l[r_p \Delta_p (1 - (r_p/R)^{2l})]^{-1}, & l \neq 0; \end{cases} \quad (2.1.5)$$

with  $l$  being the azimuthal wavenumber. An azimuthally symmetric wave that obeys dispersion relation (2.1.4) with  $l = 0$  is also called a cable plasma wave [10, 21]. This wave has the highest phase velocity and thus plays an especially important role in plasma relativistic microwave electronics. In the classification accepted in the waveguide theory, this wave is designated as  $E_{01}$ . As the wavenumber increases ( $k_z R > 1$ ), the wave phase velocity (2.1.4) decreases abruptly, so that the wave acquires the nature a potential wave and becomes trapped in the plasma.

In the long-wavelength limit, the squared transverse wavenumber  $k_{\perp b}^2$  is also described by formula (2.1.5) with subscript  $b$  in place of  $p$ , in which case the spectra of both fast and slow beam waves can easily be found from the dispersion functions (2.1.2) (see [10, 19, 20] for details). A slow beam wave has negative energy, so that the beam in the plasma is unstable. The frequency at which the phase velocity of a surface plasma wave with frequency (2.1.4) coincides with the beam velocity is called the frequency of the single-particle Cherenkov resonance (the wave-particle resonance). The frequency at which the phase velocity of the plasma wave is equal to the phase velocity of the slow beam wave is referred to as the frequency of the collective Cherenkov resonance (the wave-wave resonance). One can readily show that the frequency of the single-particle resonance decreases with  $\omega_p$  and vanishes at [19, 20]

$$\omega_p^2 = \omega_{p0}^2 = k_{\perp p}^2 u^2 \gamma^2. \quad (2.1.6)$$

If the plasma frequency is below the threshold frequency (2.1.6), then the single-particle Cherenkov resonance is impossible. The threshold frequency (2.1.6) is the lowest for an azimuthally symmetric cable

plasma wave. The absence of resonance does not imply that there is no stimulated Cherenkov emission and, accordingly, that the generated microwaves are not amplified. Below, we will show that, for electron beams with sufficiently high densities, the threshold plasma frequency  $\omega_p$  is significantly below the threshold (2.1.6) [19, 20].

In a beam-plasma system, microwaves can be amplified in different frequency bands, depending on the system parameters (primarily, on  $\omega_p$  and  $|r_b - r_p|/R$ ). Thus, if the coupling coefficient is close to unity ( $\theta \approx 1$ ), then the microwaves are amplified over a broad frequency band—from nearly zero to a frequency higher than the wave-wave resonance frequency. In the literature, such broadband plasma microwave sources are referred to as Thomson amplifiers [19, 20, 24]. If the coupling coefficient is much smaller than unity ( $\theta \ll 1$ ), then microwaves are amplified in a narrow frequency band. In the literature, such narrowband plasma microwave sources are referred to as Raman amplifiers [19, 20, 22].

The frequency characteristics that are most important for the beam-plasma interaction are shown in Fig. 1 as functions of the plasma frequency  $\omega_p$ . Curves 1 and 2 are, respectively, the upper and lower boundary frequencies of the amplification band: the amplification is possible only at frequencies lying between curves 1 and 2. Curve 3 shows the frequencies at which the amplification coefficient is maximum. Curves 4 and 5 reflect the collective and single-particle resonance frequencies, respectively. All of the curves were computed for an experimental waveguide with the parameters  $R = 1.8$  cm,  $r_p = 1.1$  cm,  $r_b = 0.6$  cm,  $\Delta_b = \Delta_p = 0.1$  cm,  $I_b = 2$  kA, and  $\gamma = 2$  ( $u = 2.6 \times 10^{10}$  cm/s).

As can be seen in Fig. 1, microwaves can be amplified only when the plasma frequency  $\omega_p$  is above a certain threshold, which is marked by the vertical line A and, because of the high beam current, is lower than the threshold (2.1.6) by a factor of approximately two. For higher plasma frequencies (i.e., those lying between the vertical lines A and D), the lower boundary frequency of the amplification band is equal to zero (the zone of Thomson amplification). For even higher plasma frequencies (i.e., those lying to the right of the vertical line D), the lower boundary frequency of the amplification band becomes nonzero and the amplification band itself narrows as  $\omega_p$  increases (the zone of Raman amplification). In turn, the zones of Thomson and Raman amplification regimes can be divided into subzones (bounded by the vertical lines B, C, and E). From Fig. 1, we can also see that, as  $\omega_p$  increases, the amplification band becomes significantly narrower and the frequency at which the amplification is most efficient (curve 3) increases and eventually becomes equal to the collective resonance frequency (curve 4). Consequently, the higher the plasma frequency and the beam current, the clearer the collective nature of the beam-plasma interaction, because coefficient  $\theta$  decreases as  $\omega$  increases.

In contrast, as the plasma frequency increases, the single-particle resonance frequency (curve 5) progressively deviates from the frequency at which the amplification coefficient is maximum (curve 3). Moreover, Fig. 1 demonstrates that amplification at the single-particle resonance frequency ceases above a certain plasma frequency [19].

In Fig. 2, curve 1 shows the maximum amplification coefficient (the quantity  $\delta k = |\text{Im}(k_z)|$ ) calculated as a function of  $\omega_p$  along curve 3 in Fig. 1 for microwave sources with the same parameters as in Fig. 1. We can see that there is a certain optimum plasma frequency at which the amplification coefficient has an absolute maximum.

Figure 3 illustrates the amplification coefficients for a system with the same parameters as in the previous two figures but calculated as functions of the frequency  $\omega$  for different plasma frequencies  $\omega_p$ :  $15 \times 10^{10}$ ,  $25 \times 10^{10}$ ,  $35 \times 10^{10}$ , and  $45 \times 10^{10}$  rad/s. In this figure, curves 1 and 2 are very similar to the  $\omega$ -profiles of the amplification coefficients for a broadband Thomson amplifier, whereas curves 3 and 4 are characteristic of the Raman amplification regime.

Figures 1 and 3 and curve 1 in Fig. 2 refer to an azimuthally symmetric cable plasma mode  $E_{01}$ . The other waves described by dispersion relation (2.1.4) obey analogous dependences. The mode with the phase velocity closest to the phase velocity of the  $E_{01}$  mode is the first azimuthally asymmetric  $E_{11}$  ( $l = 1$ ) mode, whose amplification coefficient is represented by curve 2 in Fig. 2. For high plasma densities, the amplification coefficients of these two modes are approximately the same. Consequently, in terms of the transverse wavenumber  $k_{\perp p}$  defined by formula (2.1.5), the plasma microwave amplifier is not, generally speaking, a single-mode amplifier. The single-mode regime takes place only in a comparatively narrow range of plasma frequencies (as is shown in Fig. 2). The dependences displayed in Figs. 1–3 make it possible to determine (in the linear approximation) the frequency spectra of the microwave radiation and the frequency bandwidths for microwave amplification in a plasma relativistic microwave amplifier.

2.2. Nonlinear Theory of the Plasma Relativistic Microwave Amplifier

The general nonlinear equations for the electromagnetic field of an E-wave and the currents induced in the plasma and beam in a plasma relativistic microwave amplifier have the form [19, 20]

$$\frac{\partial}{\partial t} \left( \frac{1}{r} \frac{\partial}{\partial r} r \frac{\partial}{\partial r} + \frac{\partial^2}{\partial z^2} - \frac{1}{c^2} \frac{\partial^2}{\partial t^2} \right) \Psi$$

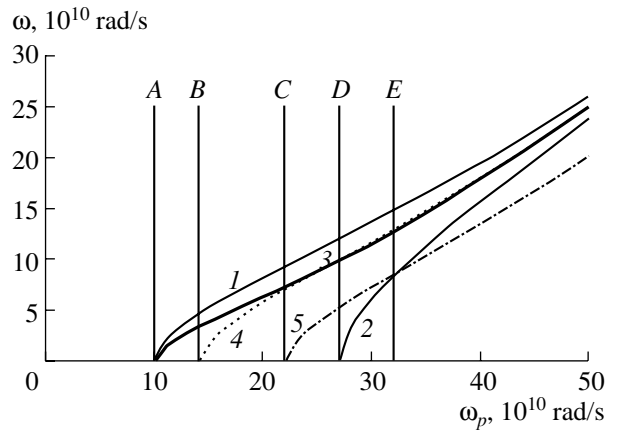


Fig. 1. The most important frequencies of a plasma amplifier vs. the plasma frequency:  $\omega_p$ : (1) upper boundary of the amplification band, (2) lower boundary of the amplification band, (3) frequency corresponding to the maximum amplification coefficient, (4) collective-resonance frequency, and (5) one-particle resonance frequency. The curves are calculated for a system with the following parameters:  $R = 1.8$  cm,  $r_p = 1.1$  cm,  $r_b = 0.6$  cm,  $\Delta_b = \Delta_p = 0.1$  cm,  $I_b = 2$  kA, and  $\gamma = 2$ .

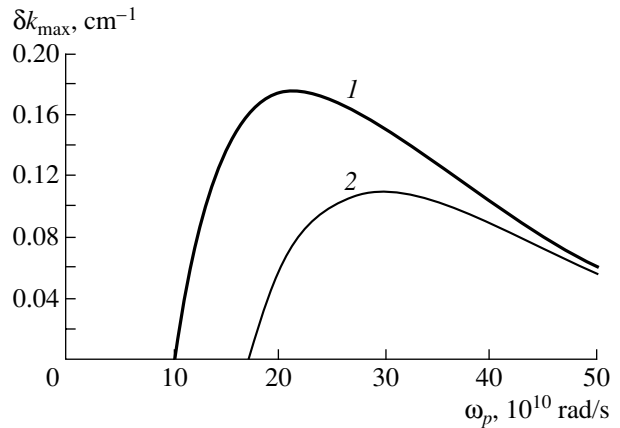


Fig. 2. Maximum amplification coefficient vs. the plasma frequency: (1) azimuthally symmetric  $E_{01}$  mode and (2) azimuthally asymmetric  $E_{11}$  mode.

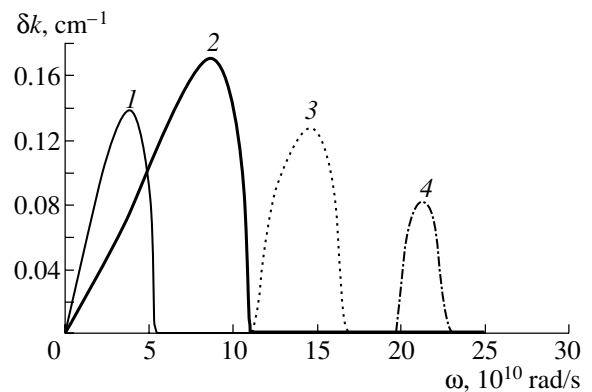


Fig. 3. Frequency dependences of the amplification coefficient for different plasma frequencies:  $\omega_p =$  (1)  $115 \times 10^{10}$ , (2)  $25 \times 10^{10}$ , (3)  $35 \times 10^{10}$ , and (4)  $45 \times 10^{10}$  rad/s.

$$\begin{aligned}
&= -4\pi(\Delta_b\delta(r-r_b)j_b + \Delta_p\delta(r-r_p)j_{pz}), \\
j_b &= en_b \int v(z, t_0)\delta[t-t(z, t_0)]dt_0, \\
\frac{\partial j_p}{\partial t} &= \frac{\omega_p^2}{4\pi}E_z, \quad E_z = \left(\frac{\partial^2}{\partial z^2} - \frac{1}{c^2}\frac{\partial^2}{\partial t^2}\right)\psi;
\end{aligned} \tag{2.2.1}$$

where  $E_z$  is the longitudinal electric field,  $\psi$  is the polarization potential, and  $n_b$  is the unperturbed density of the beam electrons. In Eqs. (2.2.1), current  $j_p$  induced in the plasma is described in the linear approximation (the effects of plasma nonlinearity and the possibility of neglecting them were considered in [23]), and the beam current  $j_b$  is determined using a model based on the calculation of the characteristics of the Vlasov equation for the beam electrons and the representation of the distribution function of the beam electrons by an integral over the initial conditions [10, 24]. In this case,  $t(z, t_0)$  and  $v(z, t_0)$  are solutions to the characteristic set of equations for the Vlasov equation,

$$\frac{dt}{dz} = \frac{1}{v}, \quad v \frac{dv}{dz} = \frac{e}{m}(1 - v^2/c^2)^{3/2}E_z, \tag{2.2.2}$$

supplemented with the initial (injection) conditions  $t(z=0) = t_0$  and  $v(z=0) = u$ . Equations (2.2.1) and (2.2.2) yield dispersion relation (2.1.1) and, hence, the remaining results of linear theory.

The general equations (2.2.1) and (2.2.2) can be reduced to a form that is convenient for solving the problem of microwave amplification with allowance for the following circumstances: (a) in a beam-plasma waveguide, the transverse structure is not known *a priori* and is established self-consistently with increasing distance from the injection plane along the  $z$ -axis; (b) the frequency spectrum of an amplified signal may not be specified *a priori*, so that it is necessary to consider the simultaneous amplification of waves with different frequencies, which interact with each other in the nonlinear stage; and (c) the longitudinal wavenumbers of the waves that are efficiently amplified by the beam are close to the wave frequency divided by the unperturbed beam velocity. These considerations allow the polarization field potential  $\psi$  to be represented as [19, 20]

$$\begin{aligned}
\psi &= \frac{1}{2} \sum_{n=1}^{\infty} \left\{ \varphi_n(\mathbf{r}_{\perp}) \right. \\
&\times \left. \sum_{s=1} \left[ A_{ns}(z) \exp\left(-is\Omega t + is\frac{\Omega}{u}z\right) + \text{c.c.} \right] \right\}.
\end{aligned} \tag{2.2.3}$$

Here,  $\Omega$  is a certain small frequency value, which serves to "discretize" the frequency spectrum of the amplified signal and is equal in order of magnitude to  $\Omega = 2\pi/T$ , where  $T$  is the characteristic time scale on which the current of an electron beam changes (the

beam pulse duration). With expression (2.2.3), Eqs. (2.2.1) and (2.2.2) reduce to the following nonlinear equations for a plasma relativistic microwave amplifier [19, 20]:

$$\begin{aligned}
\frac{dy}{d\xi} &= \eta, \\
\frac{d\eta}{d\xi} &= \frac{i}{2} \left(1 + 2\gamma^2 \frac{u^2}{c^2} \eta\right)^{3/2} \\
&\times \sum_{s=1} [s \exp(-isy) \hat{L}_s(\alpha_{bs}\rho_s + j_s) - \text{c.c.}], \\
\frac{dj_s}{d\xi} &= \frac{is}{2\gamma^2} \left[ \left(\frac{1}{\alpha_{ps}} - 1\right) j_s - \theta(s) \alpha_{bs} \hat{L}_s \rho_s \right].
\end{aligned} \tag{2.2.4}$$

Here,

$$\begin{aligned}
\rho_s &= \frac{1}{\pi} \int_0^{2\pi} \exp(isy) dy_0, \quad \hat{L}_s = 1 - 2i\gamma^2 \frac{1}{s} \frac{d}{d\xi}, \\
\alpha_{ps} &= \frac{\omega_p^2}{k_{\perp p}^2(s) u^2 \gamma^2}, \quad \alpha_{bs} = \frac{\omega_b^2 \gamma^{-3}}{k_{\perp b}^2(s) u^2 \gamma^2},
\end{aligned} \tag{2.2.5}$$

and the quantities  $k_{\perp p}^2(s)$ ,  $k_{\perp b}^2(s)$ , and  $\theta(s)$  coincide with their linear analogs correct to the replacement  $\omega \rightarrow s\Omega$ . The dimensionless parameters and variables in Eqs. (2.2.4) are defined as

$$\begin{aligned}
y &= \Omega[t(z, t_0) - z/u], \quad \eta = \frac{u - v(z, t_0)}{v(z, t_0)}, \\
y_0 &= \Omega t_0, \quad \xi = \frac{\Omega}{u} z.
\end{aligned} \tag{2.2.6}$$

The amplification efficiency is defined as a relative fraction of the kinetic energy flux of the beam electrons that is transferred into the microwave energy flux:

$$Q = 1 - \frac{1}{2\pi} \int_0^{2\pi} (1 + 2\gamma^2 (u/c)^2 \eta)^{-1/2} dy_0. \tag{2.2.7}$$

For a spatially unbounded beam-plasma system, the amplification efficiency (2.2.7) reduces to the efficiency described by formula (1.2.5) in linear theory.

Equations (2.2.4) should be supplemented with the boundary conditions. In the amplification problem, they are specified in the injection plane  $z=0$  [19, 20]:

$$\begin{aligned}
j_s|_{\xi=0} &= j_{s0}, \quad \eta|_{\xi=0} = 0, \\
y|_{\xi=0} &= y_0 + \frac{1}{2} \sum_{s=1} (b_s \exp(isy_0 + i\phi_s) + \text{c.c.});
\end{aligned} \tag{2.2.8}$$

Here,  $j_{s0}$  are the amplitudes of the current harmonics of the plasma oscillations at the entrance to an amplifier,

$y_0 \in [0, 2\pi]$  refers to an unperturbed beam, and the second term on the right-hand side of the third condition describes the electron density modulation of a beam. Generally, nonlinear theory deals with problems in which there are no plasma oscillations at the entrance to an amplifier (i.e., all of the amplitudes of the plasma-current harmonics  $j_{s0}$  are equal to zero), whereas the density of the injected beam is assumed to be weakly modulated:  $|b_s| = 0.01-0.05$ .

Below, we will present the maximum amplification efficiency, the length corresponding to the maximum output power (the optimum length), and the spectrum of the amplified signal, all obtained by numerically solving the nonlinear equations for a plasma amplifier with the same parameters as in Figs. 1-3. In order to find the maximum amplification efficiency and optimum length, it is sufficient to consider the amplification of a monochromatic signal, i.e., to use the boundary conditions (2.2.9) with only one nonzero term  $b_1 \neq 0$ , setting the remaining terms,  $b_{2,3,\dots} = 0$ , to zero. On the other hand, determining the spectrum requires taking into account many nonzero terms  $b_s \neq 0$ , which corresponds to the amplification of a large number of waves.

Figure 4 shows the maximum amplification efficiency of a monochromatic signal as a function of  $\omega_p$ , and Fig. 5 displays the optimum length  $L$  on which the maximum efficiency is achieved. These results were obtained for frequency  $\Omega$  [see formula (2.2.3)] corresponding to curve 3 in Fig. 1 and for  $b_1 = 0.01$ .

As can be seen from Figs. 4 and 5, the operation efficiency of the amplifier is fairly high over the entire range of the plasma frequencies under consideration [25] and the length of the amplifier is not too large and is essentially independent of  $\omega_p$  over a fairly broad frequency range.

The operation efficiency is especially high near the threshold for amplification [19, 20, 25], in which case the length of the amplifier sharply increases (in Figs. 4 and 5, the threshold plasma frequency  $\omega_p = 10.1 \times 10^{10}$  rad/s is shown by the vertical line). Of course, the optimum length depends on the depth  $b_1$  of the initial beam modulation, but this dependence is weak and, for a beam with a different initial modulation depth  $b'_1$ , it can be recalculated from the formula  $L' - L = \delta k^{-1} \ln|b'_1/b_1|$ , where  $\delta k$  is represented in Fig. 2.

For several plasma frequencies, Fig. 6 illustrates the spectral densities of microwave radiation at the exit from an amplifier with an optimum length corresponding to the maximum output power. The spectral density of the input signal was assumed to be uniform over the entire frequency range under consideration. Curves 1-4 were computed for the same parameters for which the relevant curves  $\delta k(\omega)$  in Fig. 3 were obtained from linear theory. We can see that, because of the nonlinear competition between different microwaves, the emission spectra are somewhat narrower than those pre-

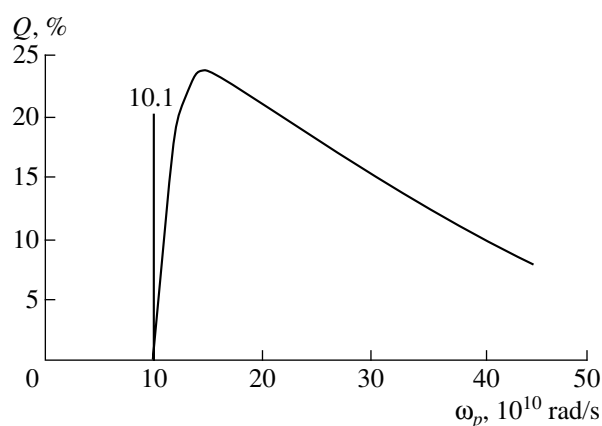


Fig. 4. Amplification efficiency  $Q$  vs. the plasma frequency  $\omega_p$ .

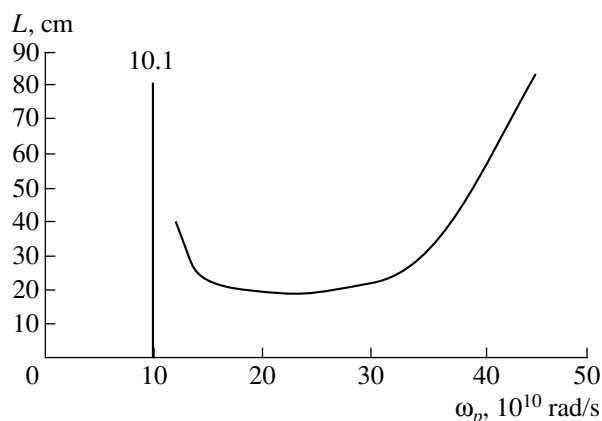


Fig. 5. Optimum accelerator length  $L$  vs. the plasma frequency  $\omega_p$ .

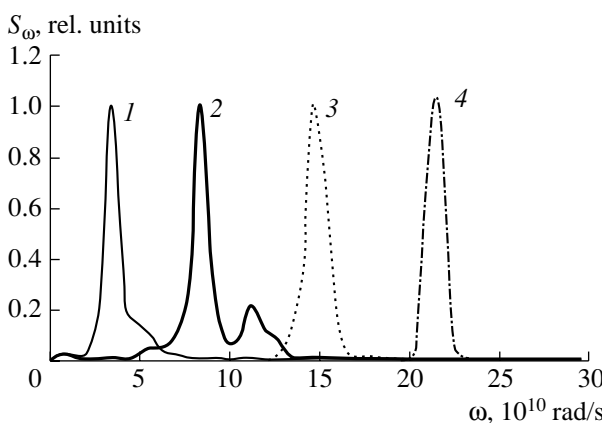


Fig. 6. Spectral density of radiation at the amplifier output for different plasma frequencies:  $\omega_p = (1) 15 \times 10^{10}$ ,  $(2) 25 \times 10^{10}$ ,  $(3) 35 \times 10^{10}$ , and  $(4) 45 \times 10^{10}$  rad/s.

dicted by linear theory. On the other hand, the maximum spectral density corresponds to the maximum in the linear amplification coefficient  $\delta k(\omega)$ . The relative

widths of the emission spectra and their central frequencies depend strongly on the plasma frequency.

### 2.3. Linear Theory of the RCPM

The theory of plasma relativistic microwave amplifier assumes that electromagnetic radiation amplified by the beam escapes freely from the amplifier through the boundary  $z = L$ . However, in reality, the plasma wave amplified by the beam is partially reflected from the exit boundary  $z = L$  and returns to the entrance plane  $z = 0$ . This effect may result in the self-excitation of the amplifier (i.e., in the start-up of microwave generation). An RCPM is usually assumed to be equipped with a metal grid that is placed at the entrance boundary  $z = 0$ , is transparent to the beam electrons, and is opaque to radiation. The exit boundary  $z = L$  of the plasma waveguide is coupled to the emitter (the outlet horn) in the form of a coaxial vacuum waveguide with an outer radius  $R$  equal to that of the plasma waveguide and with an inner radius  $r_0$  somewhat larger than the radius  $r_p$  of the plasma tube. When passing through the boundary  $z = L$ , a cable plasma wave converts into a cable vacuum wave, in which case the phase velocity of the microwave field and its structure change. As a result, the plasma wave incident on the emitting horn from the left is partially reflected.

Special numerical methods [26] developed to determine the reflection coefficients of the boundary  $z = L$  for a plasma wave in terms of the power ( $\kappa^2$ ) and amplitude ( $\kappa$ ) are based either on the direct solution of the steady-state diffraction problem or on the determination of the time during which the microwave field escapes from a plasma resonator. The reflection coefficients can also be obtained from approximate analytic formulas [27]. Since all of these approaches yield nearly the same results, the RCPM theory is constructed under the

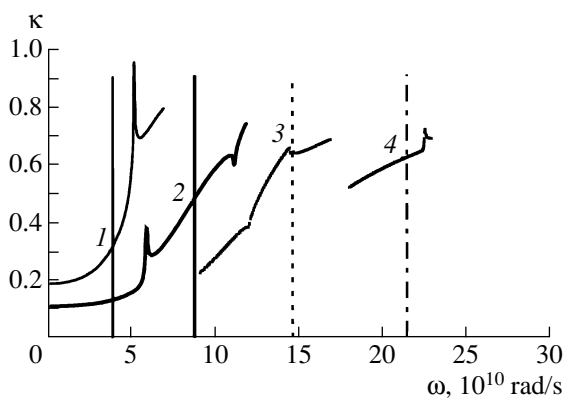


**Fig. 7.** Frequency dependences of the reflection coefficient for different plasma frequencies:  $\omega_p = (1) 15 \times 10^{10}$ ,  $(2) 25 \times 10^{10}$ ,  $(3) 35 \times 10^{10}$ , and  $(4) 45 \times 10^{10}$  rad/s.

assumption that the reflection coefficient in terms of the field amplitude,  $\kappa$ , is known. Figure 7 illustrates the frequency dependence of the reflection coefficient in terms of the amplitude, calculated for  $r_p = 1.1$  cm and  $r_0 = 1.15$  cm and for the same four values of the plasma frequency as in Figs. 3 and 6.

The vertical lines in Fig. 7 refer to the frequencies at which the amplification coefficients (Fig. 3) and the spectral densities of microwave radiation at the exit from an amplifier (Fig. 6) reach their maxima. The reflection coefficients are seen to be fairly large, although, in the cases at hand, the reflection coefficient in terms of the power,  $\kappa^2$ , does not exceed 0.5. The peaks and breaks in the profiles in Fig. 7 occur at frequencies close to any of the cutoff frequencies of the system.

The basic equations of the linear theory of the RCPM are the linearized equations (2.2.1), whose general solution in the plasma region of the system ( $0 < z < L$ ) has the form

$$\Psi = \sum_{j=1}^4 A_j \exp(ik_{zj}z), \quad (2.3.1)$$

where  $k_{zj} = k_{zj}(\omega)$  are the roots of dispersion relation (2.1.1). Since this dispersion relation is fourth-order in  $k_z$ , solution (2.3.1) contains four terms, in which constants  $A_j$  are determined with allowance for the above properties of the boundaries  $z = 0$  and  $z = L$ . This approach results in the following equation for the complex frequencies of an RCPM [10, 27]:

$$1 = \kappa(\omega) \sum_{j=1}^3 \alpha_{j4}(\omega) \exp[i(k_{zj}(\omega) - k_{z4}(\omega))L], \quad (2.3.2)$$

where  $\alpha_{j4}$  are known theoretical wave conversion coefficients at the boundary  $z = 0$  [10]. Hence, if the dependence  $\kappa(\omega)$  is known, then an RCPM can be calculated in the linear approximation by solving a complicated but purely algebraic problem (2.3.2).

The main result of linear theory is that the expression for the working frequency of an RCPM (i.e., a frequency close to the collective resonance frequency) contains an imaginary correction introduced by the energy transfer from the beam to the resonator and the escape of microwave energy through the horn [10, 27, 28]:

$$\delta\omega = i \frac{u}{2L} \left( |\text{Im} \delta k(\omega)| L - \ln \frac{q}{|\kappa(\omega)|} \right); \quad (2.3.3)$$

where  $\omega$  is the resonant frequency, the amplification coefficient  $\delta k$  is determined from Fig. 2, and  $q$  is a constant whose value lies between 2 and 3. Formula (2.3.3), which is a simplified version of a far more general expression [10, 28], is valid if  $\omega L/u \gg 1$  and the group velocity of the plasma wave is close to the beam velocity  $u$ .

Formula (2.3.3) gives the self-excitation condition for a beam-plasma resonator [19, 20, 28]:

$$|\operatorname{Im} \delta k(\omega)| L = \ln \frac{q}{|\kappa(\omega)|}, \quad (2.3.4)$$

which determines the parameters for the onset of microwave generation (usually, these are the starting beam current and starting resonator length). If the beam current and/or resonator length exceed their starting values, the amplification regime goes over to the generation regime. From Figs. 2 and 7, one can readily estimate the starting length. If the plasma frequency is not too close to the critical frequency, then the starting length is between 10 and 20 cm and equals, on the average, 15 cm. However, as can be seen from Fig. 5, the optimum length of the amplifier exceeds the starting length. Consequently, such an amplifier will operate in the generation regime. There are two ways of achieving the amplification regime: first, to make the amplifier shorter while simultaneously increasing the level of the input signal (in order to keep the efficiency optimum) and, second, to improve the coupling of the plasma resonator to the outlet horn.

#### 2.4. Nonlinear Theory of the RCPM

The general nonlinear equations for an RCPM are Eqs. (2.2.1) with the beam current  $j_b$  represented by a different expression. In the RCPM theory, the most convenient model for determining the beam current is that based on the macroparticle method, which yields [27–29]

$$j_b = en_b \frac{\lambda}{N} \sum_j v_j(t) \delta(z - z_j(t)). \quad (2.4.1)$$

Here,  $\lambda$  is a characteristic length,  $N$  is the number of macroparticles (electrons) in an unperturbed beam region of length  $\lambda$  and  $z_j(t)$  and  $v_j(t)$  are solutions to the equations of motion for the  $j$ th macroparticle:

$$\frac{dz_j}{dt} = v_j, \quad (2.4.2)$$

$$\frac{dv_j}{dt} = \frac{e}{m} (1 - v_j^2/c^2)^{3/2} E_z.$$

These equations are supplemented with the initial (injection) conditions  $z_j(t = t_{0j}) = 0$  and  $v_j(t = t_{0j}) = u$ , where  $t_{0j}$  is the time of injection of the  $j$ th macroparticle into a plasma resonator. Length  $\lambda$  is usually determined using the procedure for regularizing the delta-functions in expression (2.4.1); however, this length can also be chosen in a different way.

Clearly, the most general approach to the RCPM problem consists in direct solution of nonlinear equations (2.2.1) and (2.4.1), which should be supplemented with an additional boundary condition for the polarization potential at the open end  $z = L$  of the plasma reso-

nator. This unsteady partial condition for the emission of microwave radiation into the coaxial waveguide was stated by Bobylev *et al.* [30] and was applied to solving the RCPM problem in the most general formulation (paper [30] also contains a detailed bibliography on the subject). One of the most important results of the general nonlinear theory of an RCPM is that the spectrum of electromagnetic radiation excited during a long-term quasisteady injection of an electron beam is fairly narrow:

$$\Delta\omega \ll \omega, \quad (2.4.3)$$

which agrees with the predictions made in the nonlinear theory of a plasma microwave amplifier (Fig. 6). Of course, in the low-frequency range, in which the spectral density of the microwave radiation is described by curve *l* in Fig. 6, inequality (2.4.3) fails to hold, so that the only way to adequately describe the nonlinear regime of CPM operation is to solve the general nonlinear equations (2.2.1), (2.4.1), and (2.4.2).

Assuming that inequality (2.4.3) is satisfied, we can construct a fairly simple and very illustrative physical model that allows a detailed analysis of the main parameters of an RCPM. Based on this inequality, we consider a wave with a fixed mean frequency and a slowly varying amplitude. In particular, we use the following representation of the polarization potential of the plasma wave that accompanies (resonates with) the beam [see formula (2.2.3)]:

$$\Psi = \frac{1}{2} \sum_{n=1}^{\infty} \varphi_n(\mathbf{r}_{\perp}) \left[ A_n(z, t) \exp\left(-i\omega t + i\frac{\omega}{u}z\right) + \text{c.c.} \right], \quad (2.4.4)$$

where the amplitudes  $A_n$  vary with the  $z$  coordinate and time much more slowly in comparison with the related exponential functions. The equations for the slowly varying amplitudes can be obtained using the averaging procedure

$$\langle \Phi \rangle = \frac{1}{\lambda} \int_{z-\lambda/2}^{z+\lambda/2} \Phi(z') \exp\left(i\omega t - i\frac{\omega}{u}z'\right) dz'; \quad (2.4.5)$$

where  $\Phi$  is the quantity to be averaged and  $\lambda$  is the characteristic length in representation (2.4.1). The expression for  $\lambda$  can be found from formulas (2.4.4) and (2.4.5):

$$\lambda = \frac{2\pi u}{\omega}. \quad (2.4.6)$$

We substitute representation (2.4.4) into Eqs. (2.1.1) and (2.4.1), apply the above averaging procedure, and

perform fairly involved manipulations. As a result, we arrive at the following RCPM equations [27–29]:

$$\begin{aligned} \left(\frac{\partial}{\partial \xi} + \tilde{v} \frac{\partial}{\partial \tau}\right) J^+ &= \frac{i}{2\gamma^2} \left[ \left(\frac{1}{\alpha_p} - 1\right) J^+ - \theta \alpha_b \hat{L} \langle \rho \rangle \right], \\ \frac{dy_j}{d\tau} &= \eta_j, \\ \frac{d}{d\tau} \left( \frac{\eta_j}{\sqrt{1 - \beta^2 \eta_j^2}} \right) & \\ &= -\frac{i}{2} \gamma^3 [\exp(-i\tau + iy_j) \hat{L}(\alpha_b \langle \rho \rangle + J^+) - \text{c.c.}]. \end{aligned} \quad (2.4.7)$$

Here,

$$\begin{aligned} \langle \rho \rangle &= \frac{2}{N} \sum_j f(\tau_{0j}) \exp(i\tau - iy_j), \\ \hat{L}_s &= 1 - 2i\gamma^2 \left( \frac{\partial}{\partial \xi} + \beta^2 \frac{\partial}{\partial \tau} \right), \end{aligned} \quad (2.4.8)$$

$\theta$  is the coupling coefficient for beam and plasma waves; quantities  $\alpha_b$  and  $\alpha_p$  are defined by formulas (2.2.5); and the remaining dimensionless variables have the form

$$\begin{aligned} \tau &= \omega t, \quad \xi = \frac{\omega}{u} z, \quad y_j = \frac{\omega}{u} z_j, \quad \eta_j = \frac{v_j}{u}, \\ \beta &= u/c, \quad \tilde{v} = V_g/u, \end{aligned} \quad (2.4.9)$$

where  $V_g$  is the group velocity of a plasma wave obeying dispersion relation (2.1.4).

Although Eqs. (2.4.7) and expressions (2.4.8) are time-dependent, they exactly correspond to the above equations for the plasma amplifier, specifically, to Eqs. (2.2.4) and (2.2.5) with  $s = 1$ . Quantity  $\langle \rho \rangle$  is the complex amplitude of the perturbed beam charge density and corresponds to one of the quantities  $\rho_s$  in the equations for the plasma amplifier. In formula (2.4.8) for  $\langle \rho \rangle$ , we introduced the function  $f(\tau_{0j})$  (where  $\tau_{0j}$  is the time at which the  $j$ th electron enters the plasma resonator) in order to model the fronts and density modulation of the beam. Quantity  $J^+$  is a slowly varying amplitude of the plasma wave accompanying the beam and corresponds to one of the functions  $j_s$  in Eqs. (2.2.4).

The RCPM theory cannot be constructed only on the basis of Eqs. (2.4.7). We must also take into account the counterpropagating plasma wave, which is responsible for feedback in an RCPM. The counterpropagating wave does not resonate with the beam and, on the average, does not even interact with it. The accompanying and counterpropagating waves interact only at the side boundaries of the plasma resonator, at which they transform into one another. This transformation can be

described by the following feedback boundary condition [10, 28]:

$$J^+(\xi = 0, \tau) = -\kappa J^+(\xi = \xi^+, \tau - \xi^+/\tilde{v}), \quad (2.4.10)$$

where  $\kappa$  is the reflection coefficient introduced above,  $\xi^+ = \omega L/u$  is the dimensionless length of a plasma resonator, and the minus sign indicates that the wave phase changes as the wave is reflected from the metal grid at the boundary  $z = 0$ . Equations (2.4.7) with boundary condition (2.4.10) constitute a closed set of equations of the nonlinear RCPM theory [27–29]. The results of linear theory that were presented in Section 2.3 can naturally be obtained from the above sets of equations and the feedback condition.

Equations (2.4.7) with boundary condition (2.4.10) can be successfully used in the theory of an RCPM based on pulsed electron beams, provided that  $\omega T \gg 1$  [see condition (2.4.3)], where  $T$  is the characteristic time scale on which the beam current changes. Thus, under certain conditions during the steady injection of an electron beam, it is possible to achieve a steady-state regime of microwave generation [31], in which case we have  $\partial/\partial \tau = 0$ , so that Eqs. (2.4.7) pass over to Eqs. (2.2.4) (in which  $J^+$  should be replaced by  $j_s$ ) and the feedback condition (2.4.10) becomes

$$J^+(\xi = 0) = -\kappa J^+(\xi = \xi^+). \quad (2.4.11)$$

Equations (2.2.4) with boundary condition (2.4.11) constitute an eigenvalue problem whose solutions determine the steady-state regimes of RCPM operation. In this problem, the eigenvalue is  $J^+(\xi = 0)$ . Whether or not steady-state operation regimes exist is not *a priori* clear. However, if steady-state regimes do exist, they can be determined through a simple iteration procedure. First, for a very small value of  $J^+(\xi = 0)$ , it is necessary to solve Eqs. (2.2.4) and to determine the new value  $J^+(\xi = \xi^+)$ . Then, it is necessary to calculate the new value  $J^+(\xi = 0)$ , to solve Eqs. (2.2.4) again, and so on. If this iteration process converges, then a possible steady-state regime of RCPM operation will be determined. However, instead of iterating, one can directly look for a solution to the time-dependent equations (2.4.7) with boundary condition (2.4.10). This somewhat more involved approach makes it possible to investigate the achievement of not only steady-state but also quasi-steady-state generation regimes.

Let us consider some results of modeling an RCPM operating with a steady injection of an electron beam [31]. In the corresponding calculations, we varied the plasma frequency and the length of the plasma resonator while keeping the remaining parameters fixed:  $I_b = 2$  kA,  $R = 1.8$  cm,  $r_b = 0.6$  cm,  $\Delta_b = \Delta_p = 0.1$  cm,  $\gamma = 2$ , and  $r_p = 1.1$  cm (see above). Figure 8 shows the generation efficiency obtained as a function of the length  $L$  of the plasma resonator for the same four values of the plasma frequency as in Figs. 3, 6, and 7 and for the reflection coefficients in Fig. 7. A sharp increase in the

generation efficiency from zero to a fairly high level stems from the fact that the resonator length exceeds its starting value. As can be seen from Fig. 8, the starting lengths are very close to those determined by condition (2.3.4). In a longer plasma resonator, the generation efficiency is seen to oscillate, because the point of saturation of the beam instability is periodically displaced from the exit boundary  $z = L$  toward smaller values of  $z$  and back. In this case, the maximum values of the generation efficiency even turn out to be somewhat higher than those in the case of the amplification of a monochromatic signal. However, a comparison between Figs. 8 and 4 confirms that the generation efficiency decreases as the plasma frequency increases. On the whole, different methods and models for calculating Cherenkov plasma microwave oscillators and amplifiers based on dense electron beams yield close results on the efficiencies, spectra, critical plasma frequencies, starting characteristics, and the dependences on the main parameters of the beam-plasma system. These theoretical results agree well with the data from the experimental investigations that will be described below.

### 3. EXPERIMENTAL PLASMA RELATIVISTIC MICROWAVE ELECTRONICS

#### 3.1. Relativistic Cherenkov Plasma Maser

**3.1.1. Scheme of the RCPM.** The first experiments on the excitation of waves in a plasma waveguide by a high-current REB were carried out in 1982 [17, 18]. The RCPM scheme, which has changed insignificantly since that time, is illustrated in Fig. 9. A high-voltage pulse is applied to an accelerator cathode (1). An REB 2 is injected along the axis of a circular metal waveguide (3) prefilled with an annular plasma (4). The beam and the plasma are immersed in a uniform longitudinal magnetic field  $B$ . The beam electrons have the longitudinal velocity component only. The electron beam terminates at the end of the central conductor (5) of the coaxial emitter (6). Microwaves are generated in the plasma waveguide, propagate through the vacuum coaxial waveguide (6) and are emitted through the outlet horn (7). The basic ideas underlying this scheme are the following.

The annular plasma diameter is larger than that of the electron beam, so that the plasma does not penetrate into the diode of the high-current accelerator. In experiments on the injection of an REB into a plasma, the method of separating the diode from the plasma with the help of a thin metal foil transparent to relativistic electrons was also used. However, the use of a foil leads to the appearance of the transverse velocity component of the beam electrons, which substantially decreases the efficiency of the Cherenkov interaction.

The transverse dimensions of the waveguide, beam, and plasma, as well as the electron densities in the plasma and beam and the magnitude of the magnetic

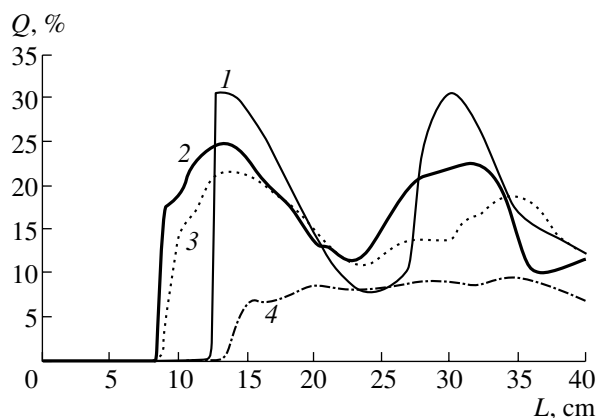


**Fig. 8.** Maximum generation efficiency  $Q$  vs. the plasma-resonator length for different plasma frequencies:  $\omega_p =$  (1)  $15 \times 10^{10}$ , (2)  $25 \times 10^{10}$ , (3)  $35 \times 10^{10}$ , and (4)  $45 \times 10^{10}$  rad/s.

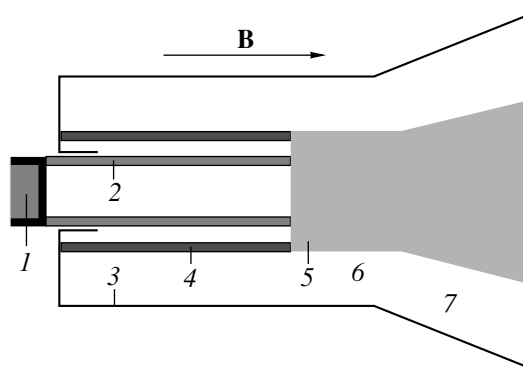


**Fig. 9.** Schematic of the RCPM: (1) accelerator cathode, (2) REB, (3) metal waveguide, (4) plasma, (5) REB collector, (6) coaxial vacuum waveguide, and (7) output horn.

field, are constant along the device axis. This circumstance significantly simplifies the theoretical analysis. The plasma is immersed in a strong uniform magnetic field such that the electron cyclotron frequency  $\Omega_e$  is higher than the microwave radiation frequency  $\omega$  ( $\Omega_e > \omega$ ). This ensures the absence of a resonant absorbing layer in which the radiation frequency is equal to the hybrid frequency:  $\omega^2 = \omega_p^2 + \Omega_e^2$ .

A substantial fraction of the energy of the excited plasma wave is concentrated inside the vacuum gap between the plasma and the waveguide wall. In this region, the field structure of the plasma wave is similar to that of the TEM mode of the coaxial outlet emitter. This fact, along with a high phase velocity close to the speed of light guarantees the high conversion efficiency of the energy of the slow plasma wave into microwave energy. The coaxial outlet emitter used in the scheme provides the efficient extraction of radiation from the RCPM in a broad frequency band.

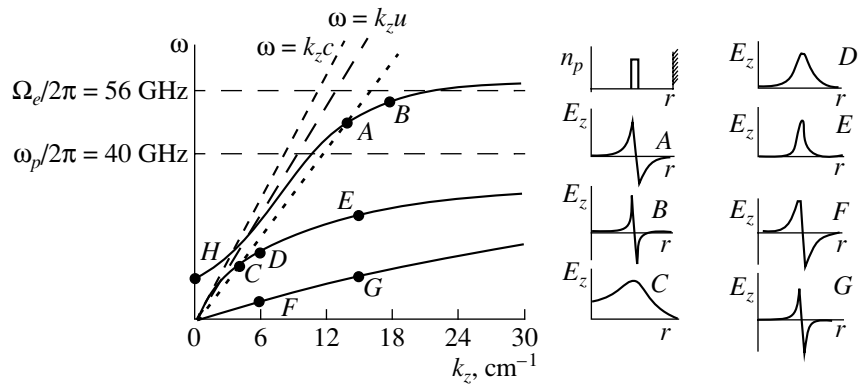


**Fig. 10.** Dispersion of modes of a plasma waveguide in a finite magnetic field at  $\Omega_e = 1.4\omega_p$  (on the left) and the radial profiles of the plasma density  $n_p(r)$  and longitudinal component  $E_z(r)$  of the microwave electric field for points A–G (on the right). Curve *HAB* corresponds to the vacuum  $E_{01}$  mode modified in the presence of a plasma; curve *OCE* corresponds to the lowest radial mode ( $i = 1$ ) of the slow azimuthally symmetric plasma wave; curve *OFG* is the same for  $i = 2$ ; and the dashed line *OCA* corresponds to the slow wave of the beam space charge.

The maximum value of  $\delta k$  in Fig. 3 at fixed values of the electron energy and the electron beam current depends on the coupling between the beam and the plasma wave. In the experiment, the coupling was varied by varying the gap length between the annular REB and plasma. As the gap length decreases, both field  $E_z$  in the electron beam (see the distribution  $E_z(r)$  at point *C* in Fig. 10) and  $\delta k$  increase.

Figure 10 shows the calculated dispersion curves for the waves in the plasma waveguide and the radial profiles of the electric field of the plasma wave for the following experimental conditions: the radius of the metal waveguide is  $R = 1.8$  cm, the radius of the annular plasma is  $r_p = 1$  cm, the plasma thickness is  $\Delta r_p = 0.1$  cm,  $\gamma = 2$ ,  $I_b = 2$  kA, and  $\Omega_e = 1.4\omega_p$ .

When the waveguide is filled with a plasma, the fast wave of the vacuum waveguide  $E_{01}$  (whose phase velocity exceeds the speed of light) is converted into the mode presented by curve *HAB*. This mode of the plasma waveguide remains fast at low frequencies, but it becomes slow as the frequency increases:  $\omega \rightarrow \Omega_e$  for  $k_z \rightarrow \infty$ . In Fig. 10 (on the right), the radial profiles of the component  $E_z$  of the microwave electric field are also shown. It is seen that, as  $k_z$  increases, field  $E_z$  becomes more concentrated inside the plasma (compare the  $E_z(r)$  profiles for points *A* and *B*).

Now, we consider the dispersion of slow plasma waves whose frequencies lie below  $\omega_p$ . Figure 10 shows the dispersion curves of two axisymmetric plasma modes *OCDE* and *OFG*. For large values of the longitudinal wavenumber  $k_z$ , the frequency  $\omega$  of both modes approaches  $\omega_p$ . The *OCDE* mode is the lowest radial mode (see the  $E_z(r)$  profiles for points *C*, *D*, and *E*), whereas the *OFG* mode is a higher radial mode (see the  $E_z(r)$  profiles for points *F* and *G*). As is the case of the faster mode represented by curve *HAB*, field  $E_z$

becomes more concentrated inside the plasma as  $k_z$  increases (compare the  $E_z(r)$  profiles for points *C* and *E* and points *F* and *G*, respectively). This means that, at large  $k_z$  values, the wave transforms into the longitudinal wave of an infinite cold plasma with frequency  $\omega_p$  and the group velocity close to zero.

The straight line  $\omega = k_z u$  in Fig. 10 corresponds to a beam with an electron energy of 500 keV. For the finite value of the beam electron density, the dispersion curve of the slow beam wave takes the form of line *OCA*. The electron beam interacts with only one of two slow plasma waves *OCDE* and *OFG*, namely, with the lowest radial mode: curve *OCA* (electron beam) intersects curve *OCDE* (plasma) at point *C*, but does not intersect curve *OFG*. Thus, it is possible to avoid the intersection of curve *OCA* with all the curves (curve *OFG* and, maybe, other) except one (curve *OCE*), if the slope of these curves near the coordinate origin is sufficiently low. This example illustrates the principle of mode selection for the slow plasma waves: it is possible to suppress the excitation of all of the slow plasma waves except one if their group velocities are sufficiently small at  $k_z \rightarrow 0$ .

The intersection of the curves at point *A* in Fig. 10 shows that there is the possibility of coupling between the electron beam (curve *OCA*) and the wave represented by curve *HAB*. In this case, the selection of modes (the plasma wave *OCDE* and wave *HAB*) is based on another principle, namely, on the difference between the electric field profiles  $E_z(r)$  shown on the right in Fig. 10. We note that, near the waveguide axis (at small values of  $r$ ), the field  $E_z$  of the fast wave at point *A* almost vanishes. In the same region near the axis, the slow plasma wave (at point *C*) has a substantially higher amplitude of the longitudinal electric field  $E_z$ . In the case of the Cherenkov interaction with the electron beam, the wave with a higher field will pre-

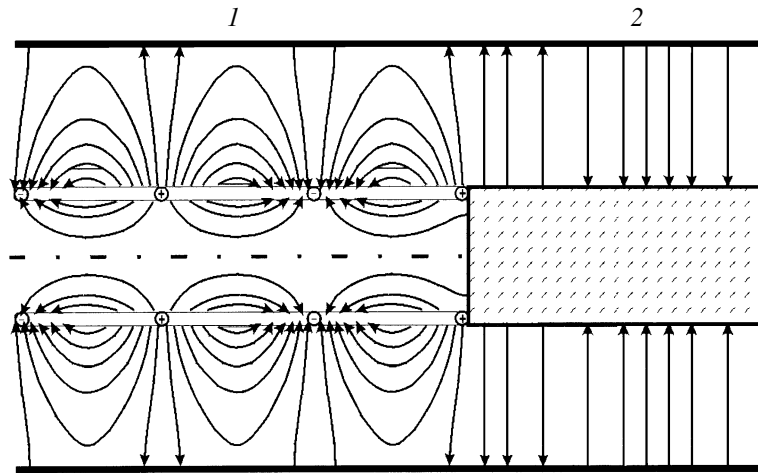


**Fig. 11.** Pattern of the electric field in a plasma waveguide for point *D* in Fig. 10: (1) plasma waveguide region, and (2) metal coaxial waveguide.

dominantly be excited. Therefore, the slow plasma wave will only be excited if the electron beam radius is not too large.

Figure 11 shows the pattern of the electric field at point *C*; this picture qualitatively confirms the  $E_z(r)$  profile presented in Fig. 10.

It can be seen in Fig. 11 that the field  $E_z(r)$  is maximum inside the plasma and decreases both toward the axis and toward the waveguide wall. It is also easy to infer that the field outside the plasma is high when the wavelength satisfies the inequality  $2\pi/k_z > R - r_p$ .

From Fig. 11, we can draw two important inferences. First, the field distribution in the gap between the plasma and the waveguide wall is similar to the field distribution of the TEM mode of a coaxial plasma waveguide. This favors the good conversion of this wave into the wave of the metal coaxial waveguide, through which microwave energy is emitted into space. Second, the field at the wall of the metal waveguide is relatively low (particularly, at short wavelengths) and has the radial component only. This circumstance, along with the presence of a strong external longitudinal magnetic field, decreases the probability of microwave breakdown on the waveguide wall.

The frequency dependence of the electric field amplification coefficient  $\delta k$  for different values of the plasma density was given above in Fig. 3. It is seen that, for a fixed value of the plasma density, the linear theory predicts the broadband microwave excitation. An important point is that, over a wide range of plasma densities, the maximum value of the amplification coefficient varies only slightly within a wide frequency band (in our case, from 12 to 20 GHz). This shows promise for creating an oscillator (or amplifier) in which a broadband frequency tuning at a constant efficiency will be achieved by only varying the plasma density, without changing the geometry of the device.

**3.1.2. Experimental Results and Comparison with Theory.** Typical parameters of RCPMs are the following. In different experiments [17, 32–35], the radius of the metal waveguide was in the range  $R = 18\text{--}35$  mm, the waveguide length was  $L = 10\text{--}50$  cm, the REB radius was  $r_b = 6\text{--}14$  mm, and the plasma radius was  $r_p = 7\text{--}20$  mm. The plasma waveguide was in a uniform magnetic field  $B = 1.7\text{--}2.2$  T. The energy of beam electrons was in the range 500–700 keV; the beam current was  $I_b = 2\text{--}3$  kA; and the current pulse duration in different experiments was 30, 100, or 1000 ns.

The fact that confirms the Cherenkov mechanism for the plasma wave excitation is the presence of a threshold plasma density [see formula (1.2.8)] above which microwave radiation is generated. For comparison, the experimental [35] and calculated values of the threshold plasma density are presented in the table for two plasma resonator lengths  $L = 10$  and 20 cm. The other parameters are the following:  $R = 1.8$  cm,  $r_p = 1$  cm,  $r_b = 0.6$  cm,  $\Delta_p = \Delta_b = 0.1$  cm,  $\gamma = 2$ , and  $I_b = 2$  kA.

Taking into account the measurement accuracy and the inevitable difference between the experiment and the theoretical model, we can conclude that the table demonstrates quantitative agreement between calculations and experiment.

Figure 12 shows the RCPM spectra [35] for  $R = 1.8$  cm,  $r_p = 1$  cm,  $r_b = 0.6$  cm,  $L = 20$  cm,  $\gamma = 2$ ,  $I_b = 2$  kA,  $B = 2.2$  T, and different values of the plasma density. It follows from the figure that the mean microwave

Threshold plasma density

	Experiment	Calculation
$L = 10$ cm	$5 \times 10^{13} \text{ cm}^{-3}$	$2 \times 10^{13} \text{ cm}^{-3}$
$L = 20$ cm	$3 \times 10^{12} \text{ cm}^{-3}$	$2 \times 10^{12} \text{ cm}^{-3}$

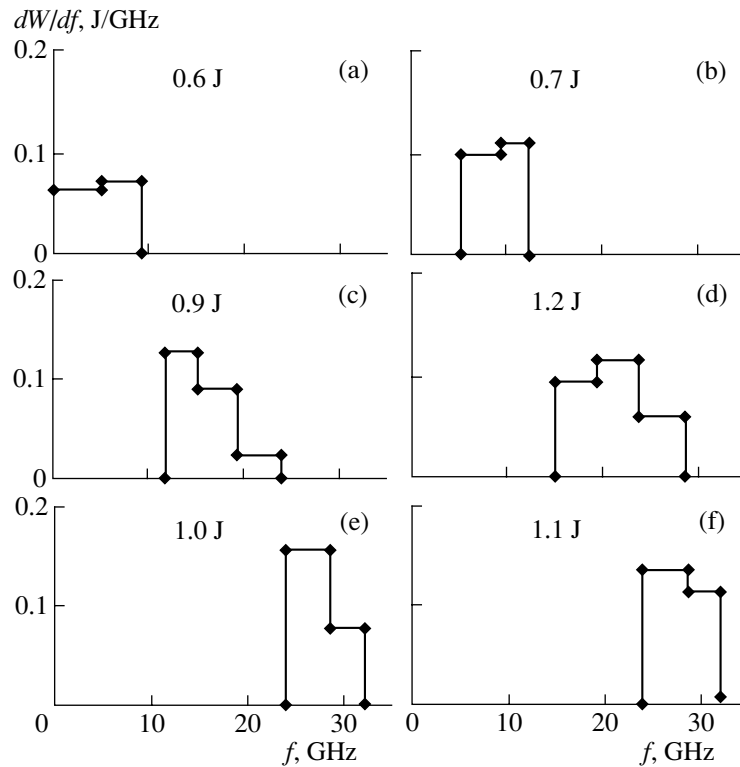


**Fig. 12.** Spectra of an RCPM for several values of the plasma density:  $n_p =$  (a)  $4 \times 10^{12}$ , (b)  $9 \times 10^{12}$ , (c)  $2 \times 10^{13}$ , (d)  $4.5 \times 10^{13}$ , (e)  $6 \times 10^{13}$ , and (f)  $7 \times 10^{13} \text{ cm}^{-3}$ . The total energy of the microwave pulse is given in each figure.

frequency increases from 4 to 30 GHz as the plasma density increases from  $4 \times 10^{12}$  to  $7 \times 10^{13} \text{ cm}^{-3}$ .

In Fig. 13, the experimental dependence of the mean RCPM frequency on the plasma density is compared with the results of calculations. Calculations were per-

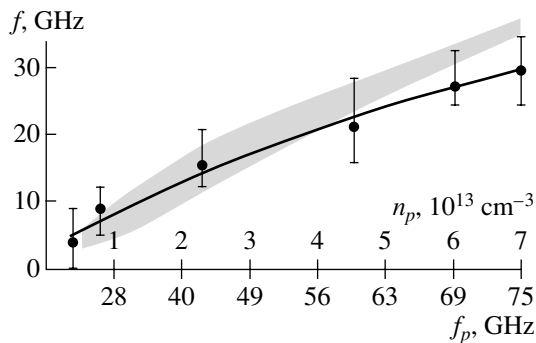


**Fig. 13.** Microwave frequency  $f$  vs. the plasma density  $n_p$  and the plasma frequency  $f_p = \omega_p/2\pi$ . The bold line and points correspond to the experiment, the vertical bars show the measured spectral width (corresponding to Fig. 12). The calculated spectrum width at a level of 0.3 of the maximum value of the emission spectral density is shown by shading. The calculation is performed for  $\Omega_e/2\pi \gg f_p$ ; in the experiment, we have  $\Omega_e/2\pi = 62 \text{ GHz}$ .

formed for an amplifier at given input frequencies from 0 to 40 GHz. We stress the fact that calculations were carried out for an amplifier; i.e., we did not take into account the possible effect of the reflection of the generated radiation from the ends of the plasma waveguide (as is in the experiment) on the emission spectrum. Nevertheless, the experimental dependence of the mean frequency on the plasma density, for the most part, coincides well with calculations; the discrepancy is only observed at high plasma densities.

The experimental spectrum width is shown in Fig. 13. However, the accuracy of measurements of the spectrum width was rather low; it may be only asserted that the spectrum width is no larger than the value given in the figure and is no less than one-half of this value. Therefore, it follows from Fig. 13 that the RCPM spectrum width is greater than or equal to the calculated value of the amplifier spectrum width. The microwave pulse duration was equal to 25 ns over the entire range of plasma densities. Consequently, 1 J corresponds to a power of 40 MW. Note that, as the plasma density varies from  $9 \times 10^{12}$  to  $7 \times 10^{13} \text{ cm}^{-3}$ , the microwave power varies insignificantly (from 30 to 50 MW) and the efficiency varies from 3 to 5%.

According to calculations (Fig. 8), the efficiency of a microwave oscillator of length  $L = 20 \text{ cm}$  varies from 13 to 8% as the plasma density varies from  $7 \times 10^{12}$  to

$6 \times 10^{13} \text{ cm}^{-3}$ . Consequently, the degree to which the calculated power is constant within this range of plasma densities coincides well with the experiment: the ratio between the maximum and minimum efficiencies is equal to 1.6. However, the experimental value of the efficiency is nearly half as large as the calculated one. According to Fig. 8, the maximum value of the calculated efficiency is achieved at a plasma resonator length of  $L = 12 \text{ cm}$ . Qualitatively the same dependence (i.e., the increase in the efficiency with decreasing length  $L$ ) was observed in the experiment: as the length decreased from 20 to 10 cm, the power increased from 50 to 60 MW and the efficiency reached 6%.

The results presented in Figs. 12 and 13 were obtained with a plasma waveguide length of  $L = 20 \text{ cm}$ ,  $B = 2.2 \text{ T}$ , and  $n_p = (0.4\text{--}7) \times 10^{13} \text{ cm}^{-3}$ , in which case we have  $\Omega_e/\omega_p = 3.5\text{--}0.82$ . We note that, in calculations, it was assumed that  $\Omega_e \gg \omega_p$ . From Fig. 13, it can be seen that the calculated and experimental data coincide at  $\omega_p < \Omega_e$ . Note that, in the experiment with a lower magnetic field of  $B = 1.2 \text{ T}$ , the coincidence between calculations and experiment was also observed at  $\omega_p < \Omega_e$ .

Hence, the characteristic experimental dependences are qualitatively confirmed by calculations (except for the absolute value of the efficiency). The coincidence of the calculated and experimental dependences of the emission frequency on the plasma density implies that, indeed, an axisymmetric lowest radial mode of the slow plasma wave is excited in the experiment. The width of the emission spectrum and the generation efficiency are determined by the frequency dependence of the linear amplification coefficient  $\delta k(\omega)$  and the nonlinear processes of trapping the beam electrons by the microwave field.

Thus, an RCPM has been created whose mean frequency can be continuously tuned over a wide band with an upper-to-lower boundary frequency ratio of 7. The frequency can be tuned during  $\sim 30 \mu\text{s}$ ; the tuning time is limited from below by the rate at which the plasma density can be varied in the electrodynamic system. Such a tuning cannot be achieved in vacuum relativistic oscillators. The maximum microwave power (0.5 GW) in our experiments was obtained by using an electron beam with an energy of 1 MeV and current of 5 kA (i.e., at an efficiency of 10%) [36].

As was mentioned in the Introduction, one of the advantages of plasma-filled microwave devices is the possibility of transporting the currents exceeding the vacuum limiting current [see formula (1.2.6)]. At the same time, calculations [28] show that the RCPM efficiency is maximum when the current is nearly half as large as the vacuum limiting current. In the experiment described above, we used a current of 2.0 kA, whereas the vacuum limiting current was equal to  $I_0 = 3.5 \text{ kA}$ . The increase in the REB current up to 3 kA [35] is not accompanied by the increase in the microwave power, which confirms the results of calculations [28].

The limiting electron beam current in RCPMs can also be increased by increasing the electron beam radius. In [32], the waveguide radius was  $R = 14.5 \text{ cm}$  and the electron beam radius was  $r_b = 10$  or  $12.7 \text{ mm}$ . The corresponding values of the vacuum limiting current were 10 and 30 kA, respectively. In this case, the diameter of the annular plasma was smaller than that of the REB and was equal to  $r_p = 7 \text{ mm}$ . For a beam with a current of 6 kA, electron energy of 420 keV, and radius of  $r_b = 12.7 \text{ mm}$ , the microwave power was  $\approx 300 \text{ MW}$ ; i.e., the efficiency attained  $\approx 12\%$ . The further increase in the current did not result in the increase in the microwave power.

For some applications, it is important to excite the  $H_{11}$  mode at the output of the microwave oscillator. In [32], a TEM-to- $H_{11}$  mode converter was installed at the RCPM output. It was shown that an REB with an electron energy of 570 keV and a current of 3 kA generated only the  $H_{11}$  mode in the emitting horn, the emission power being 100 MW and the efficiency being  $\approx$ .

**3.1.3. Microsecond RCPMs.** One of the main problems of high-power microwave electronics is the so-called "microwave pulse shortening" effect which shows up as follows. After injecting into the electrodynamic system, the REB starts to generate high-power microwaves; however, after a certain time, the generation terminates although the electron beam continues to propagate through the device. Because of the shortening effect, the duration of the microwave pulse is limited by tens of nanoseconds. This effect is the most pronounced in microwave oscillators with a relatively long duration of the current pulse (on the order of one microsecond and longer).

The cause of the microwave pulse shortening is the appearance of a plasma in different sections of the device. The plasma produced by the explosive-emission cathode expands across the magnetic field; as a result, the shape of the REB changes and the conditions for its optimum interaction with the electrodynamic structure are violated. The plasma produced at the collector bombarded by electrons expands toward the high-current REB at a velocity of up to  $10^8 \text{ cm/s}$  and can penetrate into the electrodynamic structure or merely lock-in microwaves, which thus cannot be emitted from the device. Furthermore, a plasma can be produced immediately in the electrodynamic structure by microwave breakdown.

Our long-term investigations permitted us to resolve the problem of the cathode plasma. We have created an original magnetically insulated diode [37, 38] in which the shape of an annular thin-walled REB formed at an explosive-emission cathode remained unchanged for one millisecond. It turned out that the diode also had other advantages. Using the method developed by us [39] for measuring the transverse velocities of relativistic electrons in a strong magnetic field, we revealed that their pitch angles did not exceed several degrees over the entire cross section of the dense electron beam

throughout the entire microsecond current pulse. This means that such an electron beam completely satisfies all the requirements for using it in high-power long-pulse microwave oscillators.

We have also created an original collector unit with unique properties [40]. This unit not only completely protects the oscillator from the penetration of the collector plasma into it, but also acts so that relativistic electrons reflected from the collector do not propagate along the magnetic field lines backward into the electrodynamic structure.

The most serious problem associated with the microwave pulse shortening effect is the generation of a plasma on the walls of the electrodynamic structure. We have revealed the mechanism for the formation and accumulation of this plasma [41]. This mechanism is as follows. When passing through the electrodynamic structure, the electron beam is partially degraded under the action of the strong microwave field. A relatively small fraction of electrons fall onto the wall. Nevertheless, the bombardment of the wall by electrons initiates the formation of a plasma, whose amount increases rapidly due to the surface microwave discharge on the wall.

The unique possibility of decreasing the number of electrons arriving at the wall and increasing the microwave pulse duration is to increase the distance between the electron beam and the surface of the electrodynamic structure. Unfortunately, in vacuum high-current electronics, the possibility of increasing this distance is strongly limited by the electron-beam space charge (which also determines the REB vacuum limiting current [11]). Indeed, as the distance increases, the electrostatic potential of the beam increases and the kinetic energy of electrons and, consequently, the microwave power decrease. In actual high-current electronic devices, the gap between the electron beam and the metal wall usually does not exceed several millimeters.

Thus, there is a mechanism limiting the microwave pulse duration. This effect is difficult to avoid in vacuum relativistic electronic devices; however, this problem can be resolved in plasma electronics.

As was mentioned above, the electron beam in a coaxial RCPM (Fig. 9) is shielded from outside by a dense plasma that is placed at a short distance (on the order of several millimeters) from the beam. In this case, the electrostatic field of the REB does not penetrate into the plasma. Both the electron beam and the plasma can be placed inside a metal waveguide with an arbitrarily large radius, in which case the REB electrons cannot reach the wall. In addition, the electric component of the microwave field decreases rapidly with distance away from the plasma (Fig. 10) and the electric field amplitude at the waveguide wall is much less than that in the plasma-beam coaxial line. Therefore, in the RCPM, it is relatively easy to avoid one of the main causes of the microwave pulse shortening—microwave breakdown on the wall of the electrodynamic structure.

Increasing the waveguide cross section is one of the traditional ways of decreasing the microwave field amplitude and, consequently, the probability of breakdown. In vacuum microwave electronics, this problem involves difficulties because efforts to suppress the generation of modes other than the main oscillation mode (the so-called “multimode oscillation”) are not always successful. The described structure of the microwave field in the RCPM provides an opportunity to avoid multimode oscillation, which arises when increasing the waveguide radius, and obtain a single-mode generation over a broad frequency band.

The advantages using a plasma were realized in an RCPM designed by us [42]. In this device, we used a microsecond REB (500 keV, 2 kA, 1000 ns) to obtain microwave pulses with a duration of 800 ns at a power of 40 MW.

### 3.2. Plasma Relativistic Microwave Amplifier

Experiments with the RCPM demonstrated its unique property: the possibility of varying the microwave generation frequency over a wide range (4–28 GHz) by varying the plasma density at an almost constant microwave power. The broad spectrum of the RCPM (~30% of the mean frequency) is of interest for solving a number of applied problems. However, the creation of monochromatic microwave sources that can be tuned over a frequency range as wide as in RCPMs is also of great practical importance.

The problem of the amplification of a monochromatic signal is the simplest for theoretical consideration and allows a detailed theoretical description. Therefore, it was reasonable to begin experimental studies with investigations of a plasma relativistic microwave amplifier rather than of an oscillator. However, the experimental implementation of a microwave amplifier occurred to be very complicated. The reason is the self-excitation of the device, i.e., the change of the amplification operating mode to the generation mode. The amplification of the microwave field over a broad frequency band and the simultaneous suppression of self-oscillations turned out to be a very laborious problem. That is why experiments on the plasma relativistic microwave amplifier have only been performed recently [43, 44].

**3.2.1. Scheme of the Microwave Amplifier.** The scheme of a plasma relativistic microwave amplifier [44] is shown in Fig. 14. An annular plasma (1) with a mean radius of  $r_p = 7.5$  mm and thickness of  $\Delta_p = 1$  mm is immersed in a uniform longitudinal magnetic field  $B = 1.6$  T in a cylindrical metal waveguide (2) of radius  $R = 22$  mm. A hollow thin-walled REB (3) with an electron energy of 550 keV, a current of 1.5 kA, and a pulse duration of 150 ns propagates along the waveguide axis. The mean radius of the electron beam is  $r_b = 10$  mm, and the beam thickness is  $\Delta_b = 1$  mm.

At the amplifier input, there is a microwave converter (4) exciting the TEM mode, which is converted into a fast and slow eigenmodes of the plasma waveguide (Fig. 10). The slow plasma wave is amplified by the REB. Then, it is converted into the TEM mode of the output metal coaxial waveguide and the latter is emitted by an output coaxial horn (5) with a large cross section. The plasma waveguide length over which the REB interacts with the plasma is 29 cm.

A microwave absorber (6) with an outer radius of 22 mm, an inner radius of 11.5 mm, and a length of 14 cm is placed at a distance of 3 cm from the conical collector of the REB at the outlet from the system. The absorber is intended to prevent the self-excitation of the device. The microwave absorption coefficient is equal to 20 dB for the TEM mode of a coaxial waveguide with an inner radius of 5 mm and an outer radius of 22 mm, and it is equal to 50 dB for the  $TM_{01}$  mode of a circular waveguide with a radius of 22 mm. The measurements were conducted at a frequency of 9.1 GHz.

As a source of input microwave signals, we used one of two pulsed magnetrons. One of them had a frequency of  $f_1 = 12.9$  GHz, pulse duration of 2  $\mu$ s, and power of  $P_{in} = 75$  kW. The parameters of the second magnetron were  $f_2 = 9.1$  GHz, 20  $\mu$ s, and 40 kW, respectively.

The output microwave power and the emission spectrum were measured by two detectors installed in a  $23 \times 10$  mm<sup>2</sup> receiving waveguide. The first (broadband) detector measured the total microwave power in the receiving duct. At the input of the second (narrowband) detector, there was one of two narrowband microwave filters tuned to the magnetron frequency; the filter passband was  $\Delta f = 0.29$  GHz for  $f_1 = 12.9$  GHz and  $\Delta f = 0.51$  GHz for  $f_2 = 9.1$  GHz. Both detectors had nearly the same sensitivity. When the emission spectrum was narrower than the microwave filter passband, the ratio between the signals from the narrowband and broadband detectors was equal to unity. When the emission spectrum was wider than the microwave filter passband, this ratio decreased. In this way, we could estimate the spectrum width of the output microwave radiation.

**3.2.2. Experimental Results.** Figure 15 shows the ratio between the signals from the narrowband and broadband detectors 75 ns after the REB has started to be injected into the amplifier. It can be seen that, in the range of plasma densities  $5.5 \times 10^{12} < n_p < 1.5 \times 10^{13}$  cm<sup>-3</sup>, the output signal of the microwave amplifier always lies within the passband of the narrowband detector (the power ratio is close to unity). The power of the amplified signals in this range of plasma densities always exceeded a level of 3 MW, the maximum power being 8 MW.

A comparison of the experimental dependence  $P/P_f$  (Fig. 15a) with the calculated dependence for the single-pass linear power amplification coefficient  $K$  on the plasma density (Fig. 15b) shows that the effect of

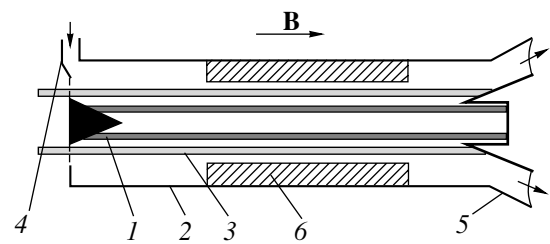


**Fig. 14.** Schematic of the plasma relativistic microwave amplifier: (1) plasma, (2) metal waveguide, (3) REB, (4) amplifier inlet, (5) coaxial conical emitting horn, and (6) microwave absorber.

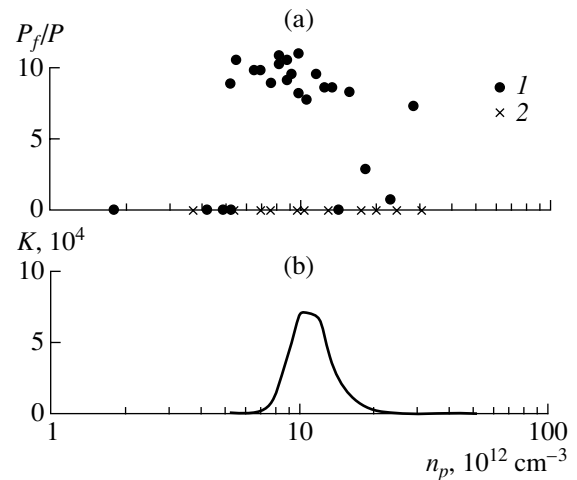


**Fig. 15.** (a) Ratio of the powers measured by the narrowband  $P_f$  and broadband ( $P$ ) detectors at a frequency of  $f_2 = 9.1$  GHz (1) in the presence of an input signal with a power of 40 kW and (2) in the absence of an input signal; (b) single-pass linear power amplification coefficient  $K$  as a function of the plasma density  $n_p$ .

microwave amplification takes place for the range of plasma densities predicted by the theory.

We note that, in the absence of an input microwave signal, no microwave radiation was detected in this range of plasma densities. This means that Fig. 15 demonstrates the amplification effect, rather than another well-known effect—the narrowing of the spectrum of a microwave oscillator under the action of an external controlling monochromatic signal.

Calculations show the frequency of the amplified radiation can be tuned over a broad band (Fig. 3). To verify this theoretical result, we also carried out experiments on microwave amplification at the frequency  $f_1 = 12.9$  GHz ( $P_{in} = 75$  kW). At this frequency, amplification was observed for higher plasma densities, namely, in the range  $10^{13} < n_p < 3 \times 10^{13}$  cm<sup>-3</sup>, which coincides with the calculation results.

Thus, a stable amplification regime was obtained for the first time for the slow plasma wave in a beam—

plasma system. It is shown that, at an input signal frequency of 9.1 GHz, there is a range of plasma densities for which the spectrum of output microwave radiation lies within the 0.5-GHz band during the entire period of REB propagation through the plasma (150 ns). The output power of the amplified signals attains 8 MW, and the power amplification coefficient is on the order of 200. It was experimentally demonstrated that the same device can also operate at a frequency of 12.9 GHz. The experiment has confirmed the theoretical prediction that there is a plasma density value at which the beam-plasma system amplifies radiation at both frequencies.

## 4. EXPERIMENTAL TECHNIQUES

### 4.1. Diagnostic of a High-Current REB and High-Power Pulsed Microwave Radiation

A high-current relativistic electron flow is a specific medium that had no analogues in the experimental physics until the advent of high-current accelerators in the early 1970s. Of course, voltages of hundreds of kilovolts and powers of several gigawatts had been used before in electrical power engineering. However, these were slowly varying (50 Hz) voltages and the power was transferred with the help of facilities tens of meters in size. Nanosecond current pulses can be generated using relatively small-sized devices; however, the requirements on the electric strength remain as stringent as earlier.

These mutually contradictory requirements, namely, that the devices should be compact and could withstand voltages up to hundreds of kilowatts and carry kiloampere currents, determine the specifics of the facilities employed in high-current relativistic electronics, in particular, the diagnostic equipment. For this reason, it was necessary to develop special methods for measuring the parameters of high-current REBs.

Concurrently, methods for diagnosing microwave pulses of unique (for those times) power (on the order of  $10^8$  W) generated with REBs were developed.

**4.1.1. Diagnostics of a High-Current REB.** In the first place, the complex diagnostics of a high-current REB includes the measurements of the electron energy (the absolute value of the electron velocity) and the total current of an electron beam. Another important parameter is the distribution of the electron current over the beam cross section. Moreover, since the electron beam propagates in the magnetic field, it is also no less important to have information about the direction of the electron velocity with respect to the field.

The total electron energy depends on the potential of the accelerator cathode, at which the electron beam is produced. The cathode potential was measured with a capacitive divider. However, in order to be convinced that the diode of the high-current accelerator indeed forms a monoenergetic electron beam and also to calibrate the capacitive divider, the electron energy was

measured directly (in absolute units) with the help of an original electrostatic analyzer [45].

The total electron beam current is difficult to measure because it is fairly high (several kiloamperes) and the current pulse is rather short. To resolve this problem, we designed special shunts made of metal conductors [46, 47] and low-inductance shunts based on conducting rubber [48].

The spatial and temporal uniformity of the electron current density over the beam cross section is the key requirement for various devices of high-current relativistic electronics. In all of our experiments, an explosive-emission cathode was used to generate the REB. The plasma emitter of this cathode varies with time, which can result in the variations in the electron beam size. To measure the distribution of the electron beam current density over the beam cross section, we designed a sectioned current-density meter [49] using a slit diaphragm.

The REB phase portrait depends on the electron kinetic energy and the orientation of the electron velocity relative the magnetic field, along which the beam propagates. The pitch angle is the angle between the electron velocity and the magnetic field. At a fixed value of the cathode potential, it is the pitch angles of electron trajectories that determine the efficiency with which the electron beam is used during plasma heating, microwave generation, etc. The development of the methods for measuring the pitch angles of electron trajectories is the most important component of the REB diagnostics.

Our first experiment on the measurements of the electron distribution over pitch angles with the help of the so-called "pinhole method" was described in [50]. In [51], for the first time, this method was grounded theoretically and a criterion of its applicability was determined. The use of rapidly varying magnetic fields allowed us to further improve this method and substantially increase the accuracy of measurements [52]. In addition, the domain of applicability of the method was extended so that it became possible to perform measurements in stronger magnetic fields and longer (by one order of magnitude) electron current pulses.

We also mention a unique method for visualizing the electron trajectories [53], which is based on the glow of a thin dielectric film under the action of relativistic electrons penetrating through it. This method allowed us to carry out the first simultaneous measurements of the electron energy and the transverse size of the beam and estimate the angular distribution of particle trajectories simultaneously at different points over the beam cross section.

**4.1.2. Diagnostics of High-Power Microwave Pulses.** The methods for measuring the parameters of microwave pulses produced with high-current REBs differ substantially from the methods that existed before the advent of gigawatt microwave electronics. In the first place, the requirements on the electric strength

of the facilities have changed, because the microwave field amplitude in relativistic microwave electronic devices attains  $10^6$  W/cm. Certain difficulties arise from the short pulse duration. Moreover, microwave pulses are usually generated in individual shots; i.e., the pulses appear rather rarely (one pulse per several minutes). The latter circumstance, as well as the rather high cost of each microwave pulse, makes it necessary to search for techniques capable of measuring all the parameters of the generated microwave radiation during a single pulse. Original methods developed by us make it possible to trace the behavior of microwave radiation throughout the entire pulse and resolve the spatial structure of radiation.

For a number of reasons, conventional semiconductor microwave detectors are difficult to use to record high-power radiation pulses in high-current microwave devices. First, they do not withstand overloads. Second, they produce too weak response signals that are difficult to discriminate against the stray background that unavoidably arises during the operation of high-current accelerators. To study the time characteristics of microwave radiation, an original method for measuring the microwave pulse envelope was proposed in [54] (and then improved in [55]). The method is based on the effect of "hot electrons" in semiconductors. A special semiconductor monocrystal does not break down at almost any incident microwave power and reproduces the shape of the microwave pulse envelope with an accuracy of up to  $\approx 1$  ns, the signal amplitude being from tens to hundreds of volts. This instrument allows the direct detection (without preliminary attenuation) of the microwave power in a waveguide at a level of hundreds of kilowatts and substantially increases the accuracy and reliability of measurements. At present, this method is standard in both Russia and other countries.

An important microwave characteristic is the wave mode. We have proposed an original method for determining the wave mode [56] from the trace produced by the microwave pulse on a dielectric surface with a special coating. As compared to the other ways of visualizing the microwave mode (e.g., a thermovisor, a panel of gas-discharge lamps, etc.), this method has an important advantage: we have a direct print of a nanosecond microwave pulse and need no additional equipment.

The methods described above allow us to trace the spatial and temporal characteristics of the microwave field, but do not ensure a sufficient accuracy in determining the total microwave energy. In the early experiments, the procedure of calculating the power was the following. The microwave power was measured (in relative units) in different points over the cross section of the radiation flow with the help of a microwave detector (see, e.g., [55]). Then, the detector was calibrated with a reference microwave source whose frequency was close to the frequency of the measured radiation or the absolute microwave power density at a certain point

was measured using some method. Finally, the results obtained were recalculated to the total pulse power.

This procedure was time-consuming, required good reproducibility of experimental results, could not ensure a necessary accuracy, and, more importantly, was unsuitable for studying microwave oscillators with broad emission spectra. For this reason, we have designed an original wide-aperture broadband calorimeter [57].

The energy of a single pulse of a relativistic microwave oscillator is difficult to measure because the pulse power is high ( $\sim 100$  MW), whereas its energy is low ( $W \approx 2$  J at  $T \approx 20$  ns). Because of the high pulse power, the diameter of the window through which the generated radiation is output from the vacuum chamber into atmosphere should be sufficiently large in order to avoid microwave breakdown on the window surface, as well on the surfaces of microwave receivers. It follows from this that the calorimeter surface should be also large; in view of this circumstance, the problem of detecting low microwave energy by a large-area (large-volume) absorber arises.

This problem was successfully resolved in [57]: a microwave calorimeter with a diameter of 40 cm and sensitivity of 0.05 J was created. The calorimeter was situated in atmosphere behind the emitting microwave horn. The operation principle of the calorimeter is to detect how the volume of an absorbing liquid increases under the action of microwave radiation. It is important that the calorimeter has nearly the same sensitivity within a broad frequency band: the microwave absorption coefficient of the calorimeter varies from 0.8 to 0.95 as the frequency varies from 5 to 40 HGz.

With this instrument, along with the methods described above, we were able to measure the microwave power in each pulse with a sufficient accuracy and reliability, determine its absolute value, and find its distribution in space and time.

One of the most important characteristics of microwave radiation is its spectrum. The traditional methods dealing with continuous or pulse-periodic radiation are of little use for measuring the radiation frequency in single short high-power pulses. We have developed and successfully used two methods for measuring microwave spectra: the local and integral ones.

The local method [58] is intended to measure the time-resolved microwave spectrum at one spatial point and is based on the use of "hot-carrier" microwave detectors [55]. Several detectors are built into low-Q resonators (necessary for measuring short pulses) fed with radiation arriving from the same resonator. This spectrometer has a relatively narrow frequency band (a few tens percent) determined by the waveguide dimensions. In this case, the instrument has all the above advantages: it is reliable, withstands overload, does not require the preliminary attenuation of the microwave power, and produces output signals on the order of tens of volts.

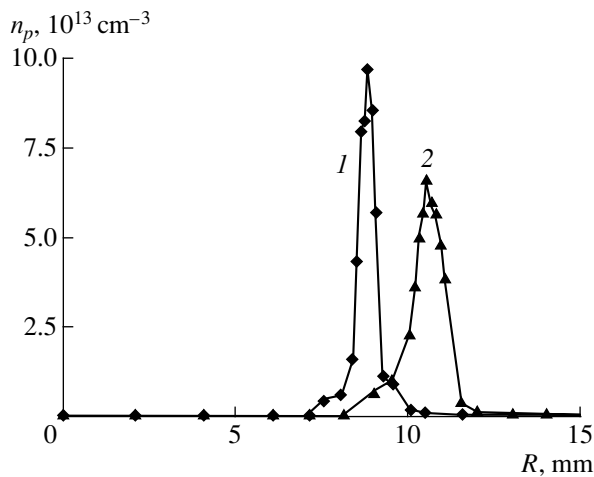


**Fig. 16.** Radial profile of the plasma density  $n_p$ : (1) magnetic field in the cathode region  $B_c$  is less than the magnetic field in the drift space  $B$  ( $B_c < B$ ) and (2)  $B_c = B$ .

The integral method is needed to measure the spectrum of the total radiation flux integrated over the microwave pulse. Such an instrument is necessary for studying a broadband microwave source (RCPM) whose mean frequency can be varied severalfold (from 4 to 30 GHz). In microwave electronics, spectral measurements are usually conducted for a small fraction of the total radiation flux. If the spectrum is broadband, then the spectral density can be different in different cross sections of the microwave beam, so that it is hardly possible to reconstruct the integral microwave spectrum from these measurements. The integral spectrum measured in absolute units (in MW/GHz) is the fundamental RCPM characteristic, which is calculated numerically and is important for applications.

To measure the integral radiation spectrum, we have designed a calorimetric spectrometer [59]. It is based on a wide-aperture calorimeter [57] that is successively masked with microwave filters with different cutoff frequencies. The filter is shaped as a disc with apertures of the same diameter; each aperture is a waveguide whose diameter determines the threshold frequency of the filter. Comparing the energy measured in two shots by the calorimeter with two filters that have different threshold frequencies, we can measure the microwave energy in the frequency range between the threshold frequencies of these filters. The calorimetric spectrometer [59] measures the energy spectrum in units of J/GHz. Independent measurements of the envelope of the microwave pulse allow us to determine the spectrum of the total radiation power in units of MW/GHz. Thus, all the parameters of high-current REBs and high-power microwave pulses were carefully measured. Often, the same parameter was measured by several methods; for the most part, we used original measurement methods; the reason is merely the absence of available alternatives to most of them.

#### 4.2. Method of Plasma Creation

The successful creation of an RCPM could be impossible if we did not find the method for creating a thin-walled annular plasma. A potential of  $-600$  V relative to the vacuum chamber wall was applied to a tungsten wire ring heated to a temperature of  $\sim 2100$  K. The tungsten cathode immersed in a strong longitudinal magnetic field created an annular electron beam whose cross section area was equal to that of the cathode. The annular electron beam ionized the gas (xenon at a pressure of  $5 \times 10^{-3}$  torr) and produced a plasma by impact ionization. However, it is hardly possible to create the plasma with a necessary density of  $10^{12}$ – $10^{13}$   $\text{cm}^{-3}$  at currents of up to 100 A and a plasma length of  $\sim 30$  cm by impact ionization only. The dense plasma was produced in a beam–plasma discharge due to the onset of the beam–plasma instability and the ionization of the gas by the microwave field. These effects are well known. A new and fundamentally important experimental fact is that the ionization by the microwave field do not increase the thickness of the annular plasma.

Figure 16 shows the radial profile of the plasma density. It can be seen that the thickness of the annular plasma is nearly equal to the thickness of the tungsten cathode wire. Due to the sharp outer plasma boundary, the diameter of the plasma is equal to that of the collector (Fig. 9). This, in turn, makes it possible to produce a transition from the plasma waveguide to the vacuum coaxial waveguide (Fig. 11) with a minimal reflection coefficient. The sharp inner boundary of the annular plasma allows us to have a narrow gap between the electron beam and the plasma and, at the same time, to ensure the absence of a plasma in the accelerator diode.

The coupling between the beam electrons and the electric field of the slow plasma wave depends on the gap length between the electron beam and the plasma. For this reason, we have developed a method for controlling the plasma diameter in the course of the experiment [60].

The possibility of varying the plasma diameter from 17 to 21 cm is demonstrated in Fig. 16. The plasma diameter is varied by the pulsed decrease in the magnetic field near the plasma source cathode. The REB was surrounded by a shield, so that the pulsed magnetic field did not penetrate into the axial region where the REB propagated. As a result, the REB propagated in a uniform magnetic field from the accelerator cathode to the collector. This eliminates the possibility of pumping the transverse electron velocity of the REB in a nonuniform magnetic field.

The plasma source operated in the pulsed mode and was switched on usually 30  $\mu\text{s}$  before the accelerator current pulse. The plasma density at the time the beam current was switched on could be controlled by varying the delay time between switching on the plasma source and the accelerator and by varying the gas pressure or the plasma-source current.

It turned out that the plasma source had a disadvantage: the annular plasma was azimuthally nonuniform. It was proved experimentally that this nonuniformity was caused by the drift instability of the radially nonuniform plasma placed in the longitudinal magnetic field [60]. In particular, according to theoretical predictions, the increase in the annular plasma thickness resulted in the decrease in the measured azimuthal modulation depth. Fortunately, the azimuthal plasma nonuniformity had no effect on the RCPM efficiency and, in this sense, was unimportant.

## 5. APPLICATION OF PLASMA RELATIVISTIC MICROWAVE SOURCES IN SCIENCE AND TECHNOLOGY

The unique frequency characteristics of high-power plasma relativistic microwave sources can find wide applications in different fields of science and technology such as plasma chemistry and plasma technologies [including fusion reactors, plasma sources (plasmotrons), and plasma thrusters]. These problems were discussed in many reviews and monographs. Here, we only consider the possible applications of high-power plasma relativistic microwave sources in plasma chemistry and radiolocation.

### 5.1. Plasma Chemistry

Short high-power microwave pulses make it possible to efficiently excite electronic and vibrational states of molecules, thus increasing the rates of chemical reactions by several orders of magnitudes as compared to traditional methods. In this case, the gas temperature varies only slightly, which is very important for plasma-chemical processes involving weakly bonded reaction products, such as complex ions. The swiping of the microwave frequency can be useful, e.g., in ECR plasma-chemical reactors. In the case of a nonuniform magnetic field, the frequency swiping is equivalent to the spatial scanning of the discharge region. This makes it possible to excite a discharge in a larger volume, in particular, in a gas layer adjacent to a large-area surface, in accordance with technological requirements of modern microelectronics.

### 5.2. Radiolocation

In radiolocation, the maximum distance at which the target  $L_d$  can be located is given by the formula [61]

$$L_d = \left( \frac{P G_A^2 \sigma \lambda^2}{(4\pi)^3 P_{\min} K} \right)^{1/4} \text{ km.} \quad (5.2.1)$$

Here,  $P$  is the radar power (in W),  $\lambda$  is the wavelength (in m),  $G_A = 4\pi S_{\text{eff}}/\lambda^2$  is the antenna emission coefficient (where  $S_{\text{eff}} = \beta S_g$  is the effective antenna area,  $\beta \approx 0.5\text{--}0.7$  is the antenna utilization factor, and  $S_g$  is the

geometric area of the antenna),  $\sigma$  is the effective reflecting area of the target (in  $\text{m}^2$ ),  $P_{\min}$  is the dimensionless factor characterizing the sensitivity of the radar, and  $K \approx 5$  is the resultant loss factor.

It follows from formula (5.2.1) that, in order to locate a small-sized target with  $\sigma = 0.01 \text{ m}^2$  (this is the effective area of the reflecting surface of present-day aircrafts made by the Stealth technology) at a distance of  $L_d = 100 \text{ km}$  at  $S_g = 4 \text{ m}^2$  and  $P_{\min} = 0.1$ , the radar should have a power of  $P \approx 50 \text{ MW}$  in the centimeter wavelength range. Actually, a radar operating at this power level was successfully used to locate a long-range aircraft [62]. The plasma relativistic microwave sources provide this power level.

However, there is a problem in radiolocation that is difficult to solve using vacuum microwave sources, but it can be solved by the methods of plasma relativistic microwave electronics. This is the location of aircrafts coated with materials absorbing microwaves. The absorbing coating is applied to the surface by sputtering the microwave-absorbing materials with plasma and by implanting charge carriers or magnetic domains into the surface layer. From a variety of the microwave-absorbing materials, we can distinguish two main classes: the resonant narrowband absorbers and nonresonant broadband absorbers. The resonant coatings efficiently absorb microwaves within a relatively narrow frequency band; e.g., radiation in the X band (8–12 GHz) is absorbed completely. The broadband absorbing materials are based on composite semiconductors consisting of free charge carriers and different kinds of implanted magnetic domains. Different domains resonantly absorb microwaves at different frequencies. Consequently, to absorb microwaves in a broad frequency band, the resonant absorption bands of different domains should overlap. The materials absorbing microwaves in the 1.5- to 15-GHz frequency range are produced precisely in this way.

It is obvious that, aircrafts coated with microwave-absorbing materials can be located only with a broadband microwave source or a tunable source. It is necessary that the frequency band of the emitter be wider than the frequency band of the absorbing coating. Such broadband high-power pulses can be produced by plasma relativistic microwave sources.

## 6. CONCLUSION

In recent years, a new field of physical electronics—plasma relativistic microwave electronics—has been created. The theory has been developed and new high-power microwave sources with broadband frequency tuning—plasma relativistic microwave oscillators and amplifiers—have been designed. The unique properties of these devices distinguish them from other high-power microwave sources. The results obtained can be summarized as follows:

(i) The emission frequency of plasma relativistic microwave sources can rapidly be varied within a very wide band. An RCPM whose frequency can be continuously tuned in a band with an upper-to-lower boundary frequency ratio of 7 (from 4 to 28 GHz) at a power of 50 MW has been created. The frequency can be retuned during several tens of microseconds.

(ii) The emission spectrum width of a plasma relativistic source can be varied in a wide range. We have obtained high-power microwave radiation with a spectrum width from <5% (in a plasma relativistic microwave amplifier) to 20–100% (in an RCPM). There are no other tunable high-power microwave sources with such a wide spectrum.

(iii) The achieved level of the microwave power (0.5 GW at an efficiency of 10%) does not exceed the maximum parameters of vacuum microwave sources. However, in plasma relativistic microwave sources, it is possible to use electron currents comparable to or even exceeding the limiting current in a vacuum system of the same geometry. Moreover, the maximum efficiency of vacuum relativistic microwave sources is achieved when the current is about 20–25% of the limiting current, whereas, in plasma devices, the maximum efficiency is achieved at nearly 50–70% of the vacuum limiting current. This provides the possibility of substantially increasing the microwave power and utilizing the resources of high-current accelerators more efficiently.

(iv) We have clarified the mechanism responsible for the suppression of high-power microwave generation in relativistic microwave devices and the shortening of microwave pulses to several tens of nanoseconds. Because of the specific design of vacuum microwave oscillators, it is hardly possible to eliminate this effect. Plasma relativistic microwave devices can generate microwave pulses with considerably longer durations and higher powers.

The reliability of the results obtained is provided by unique diagnostic methods that we have developed. Among these, we should mention a wide-aperture broadband microwave calorimeter, a high-power microwave radiation spectrometer, a method for visualizing electrons in an REB, etc.

#### ACKNOWLEDGMENTS

This work was supported in part by the International Science Foundation (grant nos. MO 3000 and MO 3300), the Ministry of Industry, Science, and Technology (MIST) of the Russian Federation under the Program for Supporting Unique Devices (Cherenkov Plasma Maser device, registration no. 01-04), the Russian Foundation for Basic Research (project nos. 94-02-03437 and 97-02-16948), and the MIST Scientific Program “Physics of Microwaves” (project 1.11. Plasma Relativistic Microwave Sources with Controlled Radiation Parameters).

#### REFERENCES

1. A. I. Akhiezer and Ya. B. Faenbeg, Dokl. Akad. Nauk SSSR **69**, 551 (1949).
2. D. Bohm and E. Gross, Phys. Rev. **75**, 1851 (1949).
3. I. F. Kharchenko, Ya. B. Faenberg, R. M. Nikolaev, *et al.*, Zh. Éksp. Teor. Fiz. **38**, 685 (1960) [Sov. Phys. JETP **11**, 493 (1960)].
4. R. A. Demirkhanov, A. K. Gevorkov, A. F. Popov, and G. I. Zverev, Zh. Tekh. Fiz. **30**, 306 (1960) [Sov. Phys. Tech. Phys. **5**, 282 (1960)].
5. G. A. Bernashevskiy, E. V. Bogdanov, V. Ya. Kislov, and Z. S. Chernov, *Plasma and Electronic Microwave Amplifiers and Oscillators* (Sov. Radio, Moscow, 1965).
6. D. I. Trubetskov and L. A. Pishchik, Fiz. Plazmy **15**, 267 (1989) [Sov. J. Plasma Phys. **15**, 152 (1989)].
7. A. A. Rukhadze, Zh. Tekh. Fiz. **31**, 1236 (1961) [Sov. Phys. Tech. Phys. **6**, 900 (1962)].
8. A. A. Rukhadze, Zh. Tekh. Fiz. **32**, 669 (1962) [Sov. Phys. Tech. Phys. **7**, 488 (1962)].
9. R. I. Kovtun and A. A. Rukhadze, Zh. Éksp. Teor. Fiz. **58**, 1219 (1970) [Sov. Phys. JETP **31**, 655 (1970)].
10. M. V. Kuzel'ev and A. A. Rukhadze, *Electrodynamics of Dense Electron Beams in Plasma* (Nauka, Moscow, 1990).
11. L. S. Bogdankevich and A. A. Rukhadze, Usp. Fiz. Nauk **103**, 609 (1971) [Sov. Phys. Usp. **14**, 163 (1971)].
12. A. A. Rukhadze, L. S. Bogdankevich, S. E. Rosinskiy, and V. G. Rukhlin, *Physics of High-Current Relativistic Electron Beams* (Atomizdat, Moscow, 1980).
13. B. I. Aronov, L. S. Bogdankevich, and A. A. Rukhadze, Plasma Phys. **16**, 101 (1976).
14. M. S. Rabinovich and A. A. Rukhadze, Fiz. Plazmy **2**, 715 (1976) [Sov. J. Plasma Phys. **2**, 397 (1976)].
15. L. S. Bogdankevich, M. S. Rabinovich, and A. A. Rukhadze, Izv. Vyssh. Uchebn. Zaved., Fiz. **10**, 47 (1979).
16. L. S. Bogdankevich, M. V. Kuzel'ev, and A. A. Rukhadze, Usp. Fiz. Nauk **133**, 3 (1981) [Sov. Phys. Usp. **24**, 1 (1981)].
17. M. V. Kuzel'ev, F. Kh. Mukhametzyanov, M. S. Rabinovich, *et al.*, Zh. Éksp. Teor. Fiz. **83**, 1358 (1982) [Sov. Phys. JETP **56**, 780 (1982)].
18. M. V. Kuzel'ev, F. Kh. Mukhametzyanov, M. S. Rabinovich, *et al.*, Dokl. Akad. Nauk. SSSR **267**, 829 (1982) [Sov. Phys. Dokl. **27**, 1030 (1982)].
19. M. V. Kuzel'ev and A. A. Rukhadze, Fiz. Plazmy **26**, 250 (2000) [Plasma Phys. Rep. **26**, 231 (2000)].
20. M. Birau, M. A. Krasil'nikov, M. V. Kuzel'ev, and A. A. Rukhadze, Usp. Fiz. Nauk **167**, 1025 (1997) [Phys. Usp. **40**, 975 (1997)].
21. M. V. Kuzel'ev, F. Kh. Mukhametzyanov, and A. G. Shkvarunets, Fiz. Plazmy **9**, 1137 (1983) [Sov. J. Plasma Phys. **9**, 655 (1983)].
22. M. V. Kuzel'ev and A. A. Rukhadze, Usp. Fiz. Nauk **152**, 285 (1987) [Sov. Phys. Usp. **30**, 507 (1987)].
23. M. V. Kuzel'ev, O. V. Lazutchenko, and A. A. Rukhadze, Izv. Vyssh. Uchebn. Zaved., Radiofiz. **42**, 958 (1999).
24. M. V. Kuzel'ev and A. A. Rukhadze, Izv. Vyssh. Uchebn. Zaved., Radiofiz. **36**, 867 (1993).
25. M. V. Kuzel'ev and A. A. Rukhadze, Fiz. Plazmy **24**, 530 (1998) [Plasma Phys. Rep. **24**, 486 (1998)].

26. I. N. Kartashov, M. A. Krasil'nikov, and M. V. Kuzelev, *Radiotekh. Élektron. (Moscow)* **44**, 1502 (1999).
27. M. Birau, M. A. Krasil'nikov, M. V. Kuzelev, and A. A. Rukhadze, *Zh. Éksp. Teor. Fiz.* **111**, 1258 (1997) [*JETP* **84**, 694 (1997)].
28. M. A. Krasil'nikov, M. V. Kuzelev, and A. A. Rukhadze, *Zh. Éksp. Teor. Fiz.* **108**, 521 (1995) [*JETP* **81**, 280 (1995)].
29. M. A. Krasil'nikov, M. V. Kuzelev, and A. A. Rukhadze, *Zh. Éksp. Teor. Fiz.* **112**, 1299 (1997) [*JETP* **85**, 705 (1997)].
30. Yu. V. Bobylev, M. V. Kuzelev, A. A. Rukhadze, and A. G. Sveshnikov, *Fiz. Plazmy* **25**, 615 (1999) [*Plasma Phys. Rep.* **25**, 561 (1999)].
31. M. A. Krasil'nikov, M. V. Kuzelev, and A. A. Rukhadze, *Kratk. Soobshch. Fiz.*, Nos. 7–8, 22 (1996).
32. I. A. Selivanov, P. S. Strelkov, A. V. Fedotov, and A. G. Shkvarunets, *Fiz. Plazmy* **15**, 1283 (1989) [*Sov. J. Plasma Phys.* **15**, 744 (1989)].
33. O. T. Loza and P. S. Strelkov, in *Proceedings of the 10th International Conference on High-Power Particle Beams, San-Diego, 1994*, Vol. 2, p. 958.
34. M. V. Kuzelev, O. T. Loza, A. V. Ponomarev, *et al.*, *Zh. Éksp. Teor. Fiz.* **109**, 2048 (1996) [*JETP* **82**, 1102 (1996)].
35. P. S. Strelkov and D. K. Ul'yanov, *Fiz. Plazmy* **26**, 329 (2000) [*Plasma Phys. Rep.* **26**, 303 (2000)].
36. M. Birau, J.-M. Buzzi, Y. Caillez, *et al.*, in *Proceedings of the 23rd International Conference on Phenomena in Ionized Gases, Toulouse, 1997*, Vol. 3, p. 46.
37. P. S. Strelkov, O. T. Loza, and S. N. Voronkov, Patent RF No. 2030135 (1995); Priority from May 8, 1992; Application No. 5041576.
38. P. S. Strelkov and O. T. Loza, Patent RF No. 2061307 (1996); Priority from June 2, 1993; Application No. 93028127.
39. O. T. Loza and I. E. Ivanov, in *Proceedings of the 13th International Conference on High-Power Particle Beams, Nagaoka, 2000*.
40. O. T. Loza, P. S. Strelkov, and S. N. Voronkov, *Fiz. Plazmy* **20**, 686 (1994) [*Plasma Phys. Rep.* **20**, 617 (1994)].
41. O. T. Loza, P. S. Strelkov, and S. N. Voronkov, *Fiz. Plazmy* **20**, 418 (1994) [*Plasma Phys. Rep.* **20**, 374 (1994)].
42. O. T. Loza, P. S. Strelkov, and I. E. Ivanov, *IEEE Trans. Plasma Sci.* **26**, 336 (1998).
43. A. V. Ponomarev, P. S. Strelkov, and A. G. Shkvarunets, *Fiz. Plazmy* **24**, 53 (1998) [*Plasma Phys. Rep.* **24**, 48 (1998)].
44. A. V. Ponomarev, P. S. Strelkov, and A. G. Shkvarunets, *Fiz. Plazmy* **26**, 633 (2000) [*Plasma Phys. Rep.* **26**, 592 (2000)].
45. Yu. F. Bondar', B. M. Koval'chuk, A. M. Rybalov, and P. S. Strelkov, *Prib. Tekh. Éksp.*, No. 1, 25 (1974).
46. O. D. Klok, V. I. Kremontsov, P. S. Strelkov, and A. G. Shkvarunets, *Zh. Éksp. Teor. Fiz.* **67**, 1401 (1974) [*Sov. Phys. JETP* **40**, 696 (1974)].
47. V. I. Kremontsov, M. S. Rabinovich, A. A. Rukhadze, *et al.*, *Zh. Éksp. Teor. Fiz.* **69**, 1218 (1975) [*Sov. Phys. JETP* **42**, 622 (1975)].
48. Yu. F. Bondar', S. I. Zavorotnyoe, A. L. Ipatov, *et al.*, *Fiz. Plazmy* **8**, 941 (1982) [*Sov. J. Plasma Phys.* **8**, 528 (1982)].
49. S. N. Voronkov, O. T. Loza, A. A. Ravaev, *et al.*, *Fiz. Plazmy* **14**, 1259 (1988) [*Sov. J. Plasma Phys.* **14**, 737 (1988)].
50. P. H. de-Haan, R. N. Singh, H. J. Hopman, *et al.*, *J. Phys. E* **14**, 373 (1981).
51. P. S. Strelkov, A. G. Shkvarunets, P. Shunka, *Fiz. Plazmy* **7**, 564 (1981) [*Sov. J. Plasma Phys.* **7**, 305 (1981)].
52. O. T. Loza and I. E. Ivanov, in *Proceedings of the 13th International Conference on High-Power Particle Beams, Nagaoka, 2000*.
53. V. I. Kremontsov, P. S. Strelkov, and A. G. Shkvarunets, *Zh. Tekh. Fiz.* **50**, 2469 (1980) [*Sov. Phys. Tech. Phys.* **25**, 1447 (1980)].
54. M. D. Ræzer and L. É. Tsopp, *Radiotekh. Élektron. (Moscow)* **20**, 1691 (1975).
55. O. T. Loza and L. É. Tsopp, *Kratk. Soobshch. Fiz.*, No. 1, 8 (1982).
56. E. A. Vinogradov, V. I. Golovanov, N. A. Irisova, *et al.*, *Zh. Tekh. Fiz.* **52**, 1458 (1982) [*Sov. Phys. Tech. Phys.* **27**, 893 (1982)].
57. A. G. Shkvarunets, *Prib. Tekh. Éksp.*, No. 4, 72 (1996).
58. A. A. Rukhadze, P. S. Strelkov, and A. G. Shkvarunets, *Fiz. Plazmy* **20**, 686 (1994) [*Plasma Phys. Rep.* **20**, 617 (1994)].
59. I. L. Bogdankevich, P. S. Strelkov, V. P. Tarakanov, *et al.*, *Prib. Tekh. Éksp.*, No. 1, 92 (2000).
60. O. T. Loza, A. V. Ponomarev, P. S. Strelkov, *et al.*, *Fiz. Plazmy* **23**, 222 (1997) [*Plasma Phys. Rep.* **23**, 201 (1997)].
61. V. P. Kalinushkin, M. V. Kuzelev, I. M. Minaev, and A. A. Rukhadze, in *Physicotechnical Problems of Electrical Energy Transfer*, Ed. by A. F. D'yakov (Mosk. Énerg. Inst., Moscow, 1998), Vol. 1, p. 11.
62. B. V. Bunkin, A. V. Gaponov-Grekhov, A. S. Elchaninov, *et al.*, in *Proceedings of the 9th International Conference on High-Power Particle Beams, Washington, 1992*, p. 195.

*Translated by I. A. Kalabalyk and N. F. Larionova*

SPELL: discretize, prefilled, aircrafts